doi: 10.4149/gpb_2021008

Identification of an autophagy-related 10-lncRNA-mRNA signature for distinguishing glioblastoma multiforme from lower-grade glioma and prognosis prediction

Bo Wei[1,*], Le Wang[2,*] and Jingwei Zhao[1]

[1] *Department of Neurosurgery, China-Japan Union Hospital of Jilin University, Changchun, Jilin, China*
[2] *Department of Ophthalmology, The First Hospital of Jilin University, Changchun, Jilin, China*

Abstract. Autophagy may provide the source of nutrients for tumor cells. We aim to develop an autophagy-related signature to predict the progression from lower-grade gliomas (LGG) to glioblastoma multiforme (GBM) and prognosis. Totally, 686 differentially expressed genes (DEGs) and 73 long non-coding RNAs (DELs) were identified between GBM and LGG samples from the Chinese Glioma Genome Atlas (CGGA). Of them, 131 DEGs were intersected with autophagy genes from the Human Autophagy Database; while 54 DELs co-expressed with autophagy-related DEGs. Ten autophagy-related genes were associated with overall survival and could distinguish GBM from LGG, with the accuracy of 0.891 using CGGA dataset and 0.790 using The Cancer Genome Atlas (TCGA) dataset. The risk score was established based on these 10 genes. Patients with higher risk score were at an increased risk of developing GBM (49.7% *vs*. 21.3%; $p < 0.001$) and worse prognosis than those in low risk group. The prognostic accuracy was 0.840 and 0.744 for CGGA and TCGA dataset, respectively. Age, recurrence, isocitrate dehydrogenase mutation and risk score were independent prognostic factors and thus they were used to build a nomogram which showed the highest prognostic power. This established nomogram may aid the clinical decision making of personalized treatment.

Key words: Glioblastoma — Lower-grade glioma — Nomogram — Prognostic signature — Autophagy-related genes — Autophagy-related lncRNAs

Introduction

Glioma is the most common category of primary central nervous system tumors (Almutrafi et al. 2020; Araghi et al. 2020), accounting for approximately 35% of all burdens. Despite huge advance has been made in the diagnosis and treatment of glioma, the overall mortality is still high, which is especially obvious in the patients with high-grade gliomas (glioblastoma, GBM; 95%) relative to lower-grade gliomas (LGG, 50%) because of its aggressive and invasive nature (Ostrom et al. 2018). Therefore, it is necessary to early stratify the patients at a high risk of developing GBM to schedule individualized treatment and improve survival.

With the development of molecular biology and bioinformatics, recent studies indicated there were obvious differences in gene expression profile between GBM and LGG (Wang and Ma 2019; Wang et al. 2019a, 2019b; Wu et al. 2019; Zhang et al. 2019, 2020; Biterge-Sut 2020). Thus, identification of molecular biomarkers may be underlying approaches to distinguish GBM from LGG and predict the prognosis. This hypothesis has been demonstrated by several authors. For example, Wu et al. (2019) found lipid metabolism-related genes were differentially expressed between GBM and LGG. Nine of them were identified to serve as a classifier for stratifying different grades. Also, this nine-gene established risk score showed strong prognostic power for glioma patients [the area under the receiver operating characteristic (ROC) curve (AUC) = 0.86 for The Cancer Genome Atlas (TCGA) dataset; AUC =

Electronic supplementary material. The online version of this article (doi: 10.4149/gpb_2021008) contains Supplementary material.

* These authors contributed to this work equally.

Correspondence to: Jingwei Zhao, Departments of Neurosurgery, China-Japan Union Hospital of Jilin University, No. 126 Xiantai Street, Changchun, Jilin 130033, China
E-mail: jwzhao@jlu.edu.cn

0.82 for the Chinese Glioma Genome Atlas (CGGA) dataset (Wu et al. 2019). Wang et al. (2019a) observed the distribution of pseudogenes was significantly different between GBM and LGG samples. Five of them were shown to be associated with overall survival (OS) and used to construct the risk score. GBM had significantly higher risk scores than LGG and may be more frequently assigned into the high risk score to result in poor OS. The predictive accuracy of this risk score for 5-year OS in glioma patients was 0.876 and 0.912 using the training and validation dataset, respectively. The study of Wang and Ma (2019) revealed the gene expression patterns of necrosis-related genes were significantly different between GBM and LGG. Seven genes were correlated with the outcome of GBM/LGG patients and integrated to generate the risk score. Survival analysis suggested that GBM/LGG patients in the high-risk group had worse OS than those in the low-risk. However, the predictors for stratifying GBM and LGG and their prognosis remain rarely reported.

Autophagy is a cellular process responsible for lysosomal degradation of damaged, denatured or aging proteins and organelles. In normal cells, the activation of autophagy protects cells against toxic injury and stress, and hereby dampens malignant transformation (Li et al. 2020). However, in tumor cells, the recycled proteins and organelles produced by autophagy may be the source of nutrients and energy for tumor growth, invasion and metastasis (Yang et al. 2019; Li et al. 2020). Theoretically, autophagy-related genes may represent promising biomarkers to predict the tumor progression (such as from LGG to GBM) and poor prognosis. This speculation has been verified in some studies. Jiang and colegue detected the expression levels of autophagic protein light chain 3 (LC3) B and p62 were higher in GBM than those in LGG tissues. High levels of LC3B and p62 protein were also associated with advanced tumor stages, worse relapse-free survival (RFS) and OS in glioma patients (Jiang and Wu 2018). The results of Padmakrishnan et al. (2019) showed autophagy proteins (LC3 and beclin 1) were highly expressed in GBM compared with LGG. Patients with low LC3/beclin 1 expression had better progression free survival (PFS) than those with high expression of LC3/beclin 1. There were also several studies to investigate a prognostic signature constituted by autophagy-related mRNAs (Wang et al. 2019c; 2020a; 2020b; 2021) for glioma patients. Nevertheless, they either focused on the genes differentially expressed only between glioma and normal controls (Wang et al. 2019c, Wang et al. 2021) or did not perform the differential analysis (Wang et al. 2020b; Wang et al. 2020c). No studies used the genes differentially expressed between GBM and LGG. In addition, Luan et al. (2019) suggested long non-coding RNAs (lncRNAs) that could co-express with autophagy-related genes also had prognostic potential for glioma, but in which lncRNAs and mRNAs were also not differentially expressed.

In present study, we aimed to develop a new autophagy-related signature based on the differentially expressed genes (DEGs) and lncRNAs (DELs) between GBM and LGG. This signature may effectively diagnose GBM patients from LGG patients and predict the poor prognostic outcomes for high-risk populations (including GBM and possibly progress to GBM).

Materials and Methods

Data source

The RNA-seq expression data (fragments mapped *per* kilobase of exon per million reads mapped, level 3) and clinical information were collected from CGGA (http://www.cgga.org.cn) and TCGA (https://portal.gdc.cancer.gov) public databases. CGGA dataset (including 431 LGG and 237 GBM samples) was used as the training set; while TCGA dataset (containing 520 LGG and 152 GBM samples) was set as the testing set (ID of each sample is shown in Supplementary material, Table S1).

Identification of autophagy-related DEGs and DELs

The mRNAs and lncRNAs in CGGA and TCGA datasets were annotated by the HUGO Gene Nomenclature Committee (HGNC; http://www.genenames.org/) that assigns a unique symbol and name to 4,516 lncRNAs and 19,200 protein-coding genes (Povey et al. 2001). DEGs and DELs were identified between GBM and LGG using package limma of R (version 3.34.7; https://bioconductor.org/packages/release/bioc/html/limma.html) (Ritchie et al. 2015). False discovery rate (FDR) < 0.05 and $|\log_2 FC(\text{fold change})| > 1$ were set as the statistical threshold. Bidirectional hierarchical clustering was performed based on all differentially expressed RNAs (DERs) using package pheatmap of R (version: 1.0.8; https://cran.r-project.org/web/packages/pheatmap). The autophagy-related gene lists were downloaded from the Human Autophagy Database (HADb, http://www.autophagy.lu/), which were then compared with the DEGs to screen the overlap (that is, autophagy-related DEGs). Pearson correlation coefficients (PCC) were calculated by cor.test function (https://stat.ethz.ch/R-manual/R-devel/library/stats/html/cor.test.html) to explore the correlation between the DELs and autophagy-related DEGs. DELs with a PCC > 0.4 were defined as autophagy-related lncRNAs. The co-expression network was established based on the interaction pairs between DELs and DEGs and visualized using Cytoscape software (version 3.6.1; www.cytoscape.org/).

Function enrichment analysis

The functions of autophagy-related DEGs in the co-expression network were analyzed using the Database for

Annotation, Visualization and Integrated Discovery (DAVID) (version 6.8; http://david.abcc.ncifcrf.gov) (Dennis et al. 2003). Gene Ontology (GO) biological process terms and Kyoto Encyclopedia of Genes and Genomes (KEGG) pathways were enriched. FDR < 0.05 was considered to be statistically significant.

Development of prognostic signature

Based on the clinical prognosis information in 668 samples of CGGA, univariate Cox regression analysis was used to filter the DELs and DEGs of the co-expression network that were significantly associated with the OS. The DELs and DEGs with a log-rank $p < 0.05$ in univariate analysis were entered into the multivariate Cox regression model for identifying independent prognostic genes. Logit regression model in glm function of R was further utilized on these independent prognostic genes to identify the feature genes that could effectively distinguish GBM from LGG. The risk score model was established for each patient by combining the expression of the feature prognostic signature and their prognostic coefficients in multivariate analysis.

The patients were divided into the high-risk group and the low-risk group by selecting the median risk score as the cut-off. The prognostic differences between the two groups were analyzed by plotting Kaplan-Meier survival curve and performing log-rank test. The predictive accuracy of the autophagy-related signature was assessed by drawing ROC curve and calculating AUC. These analyses were carried out for the training dataset (CGGA) and testing dataset (TCGA), respectively.

To explore whether the risk score was independent of clinicopathological factors, univariate and multivariate Cox regression analyses were performed using the CGGA cohort. Stratification analysis was subsequently applied for clinical variables with $p < 0.05$ in multivariate analysis to further evaluate the prognostic significance of risk score. A nomogram comprising all the variables significant in the

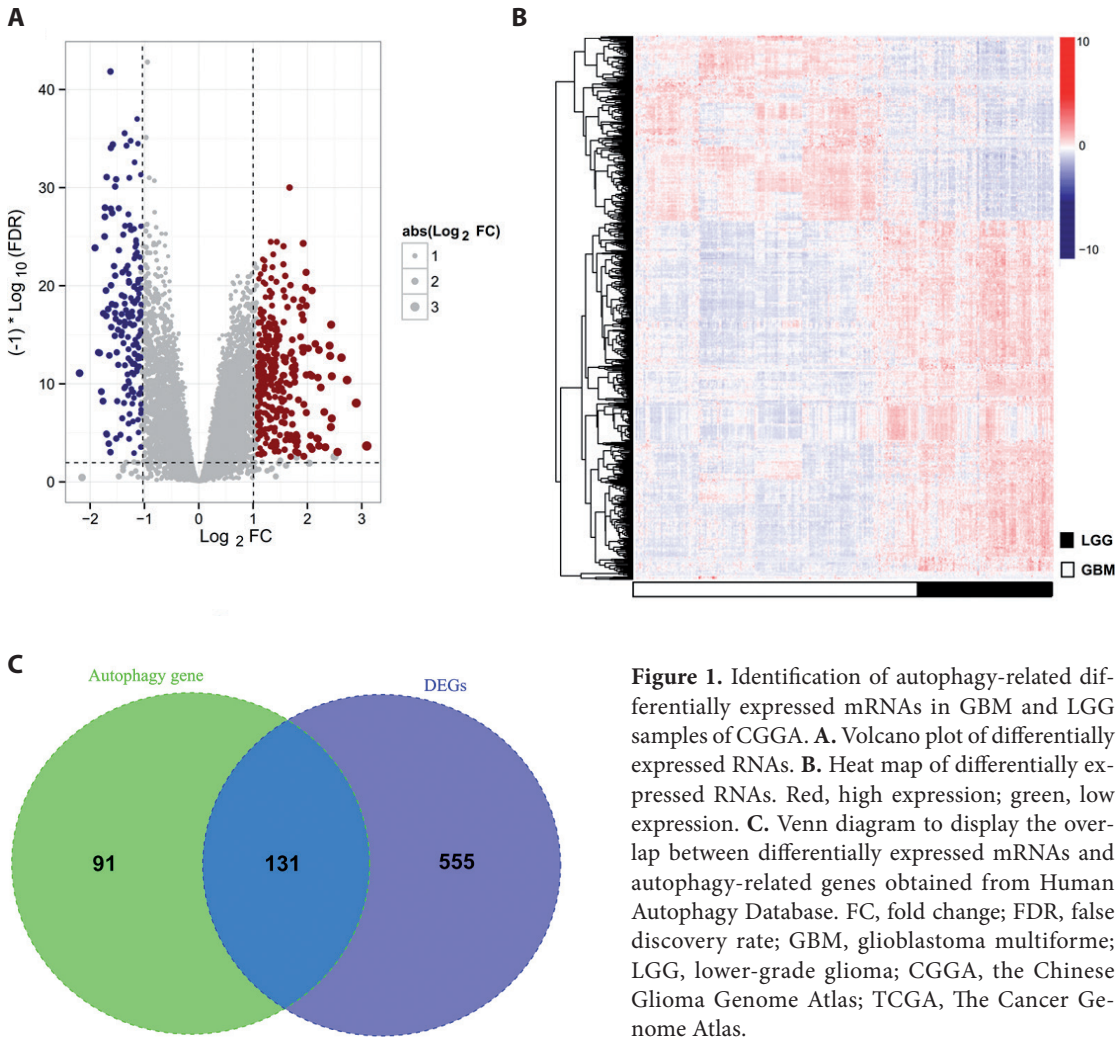

Figure 1. Identification of autophagy-related differentially expressed mRNAs in GBM and LGG samples of CGGA. **A.** Volcano plot of differentially expressed RNAs. **B.** Heat map of differentially expressed RNAs. Red, high expression; green, low expression. **C.** Venn diagram to display the overlap between differentially expressed mRNAs and autophagy-related genes obtained from Human Autophagy Database. FC, fold change; FDR, false discovery rate; GBM, glioblastoma multiforme; LGG, lower-grade glioma; CGGA, the Chinese Glioma Genome Atlas; TCGA, The Cancer Genome Atlas.

multivariate Cox regression analysis was finally generated to predict the 3-year and 5-year OS. The predictive power of the nomogram was assessed in terms of AUC, concordance index (C-index) and calibration curve.

Results

Identification of autophagy-related DERs

HGNC analysis annotated 12,350 protein-encoding mRNAs and 803 lncRNAs shared in CGGA and TCGA databases. Through LIMMA analysis of CGGA dataset, 759 RNAs (including 686 DEGs and 73 DELs) were identified to be differentially expressed between GBM and LGG (Fig. 1A). Hierarchical clustering analysis showed that GBM and LGG samples could be distinctly grouped according to the expressions of the DERs (Fig. 1B). A total of 232 autophagy-related genes were downloaded from HADb database. Venn diagrams showed 131 of them were intersected with DEGs, which were defined as autophagy-related DEGs for further analysis (Fig. 1C). After calculation of PCC, 54 DELs were considered to be co-expressed with 105 autophagy-related DEGs [such as TMEM72-AS1-ULK2 (unc-51 like autophagy activating kinase 2), WDFY3-AS2-SIRT1 (sirtuin 1)/FoxO3 (forkhead box O3)/TSC1 (TSC complex subunit 1)/HIF1A (hypoxia-inducible factor 1-alpha)] (Fig. 2), suggesting they may be autophagy-related DELs. These 131 DEGs and 54 DELs were considered as autophagy-related DERs and used for further analysis.

Function enrichment analysis for autophagy-related DEGs

To confirm the autophagy-related functions and other possible roles of our identified autophagy-related genes, function analysis was performed for the autophagy-related DEGs in the co-expression network. As expected, in 23 GO biological process terms enriched, 6 were directly involved in autophagy, including GO:0006914~autophagy [WIPI1 (WD repeat domain, phosphoinositide interacting 1), ULK2, MTOR (mechanistic target of rapamycin kinase)], GO:0016236~macroautophagy [WIPI1, MTOR, MLST8 (MTOR associated protein, LST8 homolog)], GO:0000422~mitophagy (WIPI1), GO:0000045~autophagosome assembly (WIPI1), GO:0016239~positive regulation of macroautophagy (ULK1, HIF1A), GO:0010506~regulation of autophagy (ULK1). Furthermore, these genes also regulated the apoptosis [GO:0006915~apoptotic process: NFKB1 (nuclear factor kappa B subunit 1), PPP1R15A (protein phosphatase 1 regulatory subunit 15A); GO:0043066~negative regulation of apoptotic process: MTOR, SIRT1; GO:0042981~regulation of apoptotic process: CTSB (cathepsin B)], cell cycle arrest (GO:0007050: MLST8, MTOR, PPP1R15A) and cellular response to hypoxia (GO:0071456: NFKB1, SIRT1, FoxO3, HIF1A) (Fig. 3A; Table 1). Similar to GO terms, hsa04140:Regulation of autophagy (ULK2) and hsa04210:Apoptosis (NFKB1) KEGG pathways were also enriched for co-expression network genes. In addition, several cancer signaling pathways [such as hsa05200:Pathways in cancer (NFKB1, MTOR, HIF1A), hsa04668:TNF signaling pathway (NFKB1), hsa04066:HIF-1 signaling pathway (NFKB1, MTOR, HIF1A), hsa04150:mTOR signaling pathway (ULK2, MLST8, MTOR, TSC1), hsa04068:FoxO signaling pathway (FOXO3, SIRT1), hsa04151:PI3K-Akt signaling pathway (NFKB1, FOXO3, TSC1, BCL2, MTOR, MLST8) and hsa04012:ErbB signaling pathway (MTOR)] and metabolism-related pathway [hsa05231:Choline metabolism in cancer (TSC1, MTOR, HIF1A)] were also obtained (Fig. 3B; Table 1).

Development of autophagy-related DERs-based risk score

Univariate Cox regression analysis identified 132 autophagy-related DERs (including 85 of 131 autophagy-related DEGs and 47 of 54 autophagy-related DELs) were significantly associated with OS ($p < 0.05$). Then, they were included as the variables for the multivariate Cox regression. The results showed 19 DERs (including 14 DEGs and 5 DELs) were independent prognostic factors. Logit regression model was used to further extract the feature genes that distinguished GBM and LGG from these 19 DERs. As a result, 10 genes (including 8 DEGs and 2 DELs) were obtained (Table 2). As shown in Figure 4, these 10 genes could obviously distinguish GBM from LGG, with the accuracy of 0.891 using CGGA dataset and 0.790 using TCGA dataset. Supplementary Table S2 summarized the proportion of variance of each principal component.

The risk score was calculated for each patient according to the following formula: (−2.419 × expression of TMEM72-AS1) + (−0.1293 × expression of WDFY3-AS2) + (−0.0009808 × expression of CTSB) + [−0.0002811 × expression of eukaryotic translation elongation factor 2 (EEF2)] + [−0.1031× expression of glutamate ionotropic receptor delta type subunit 2 (GRID2)] + (−0.01185 × expression of MLST8) + (0.04575 × expression of MTOR) + (−0.1039 × expression of NFKB1) + (−0.01613 × expression of PPP1R15A) + (0.04084 × expression of WIPI1). The patients were divided to two groups (low-risk group and high-risk group) using the median as the cut-off. In CGGA training dataset, it was obviously observed that patients with higher risk scores were at an increased risk of developing GBM (166/334 (49.7%) *vs*. 71/334 (21.3%); Chi-square = 59.02, $p < 0.001$). Kaplan-Meier curve analysis showed that patients in the high risk group had a significantly poorer prognosis than those in the low risk group [hazard ratio (HR) = 2.582,

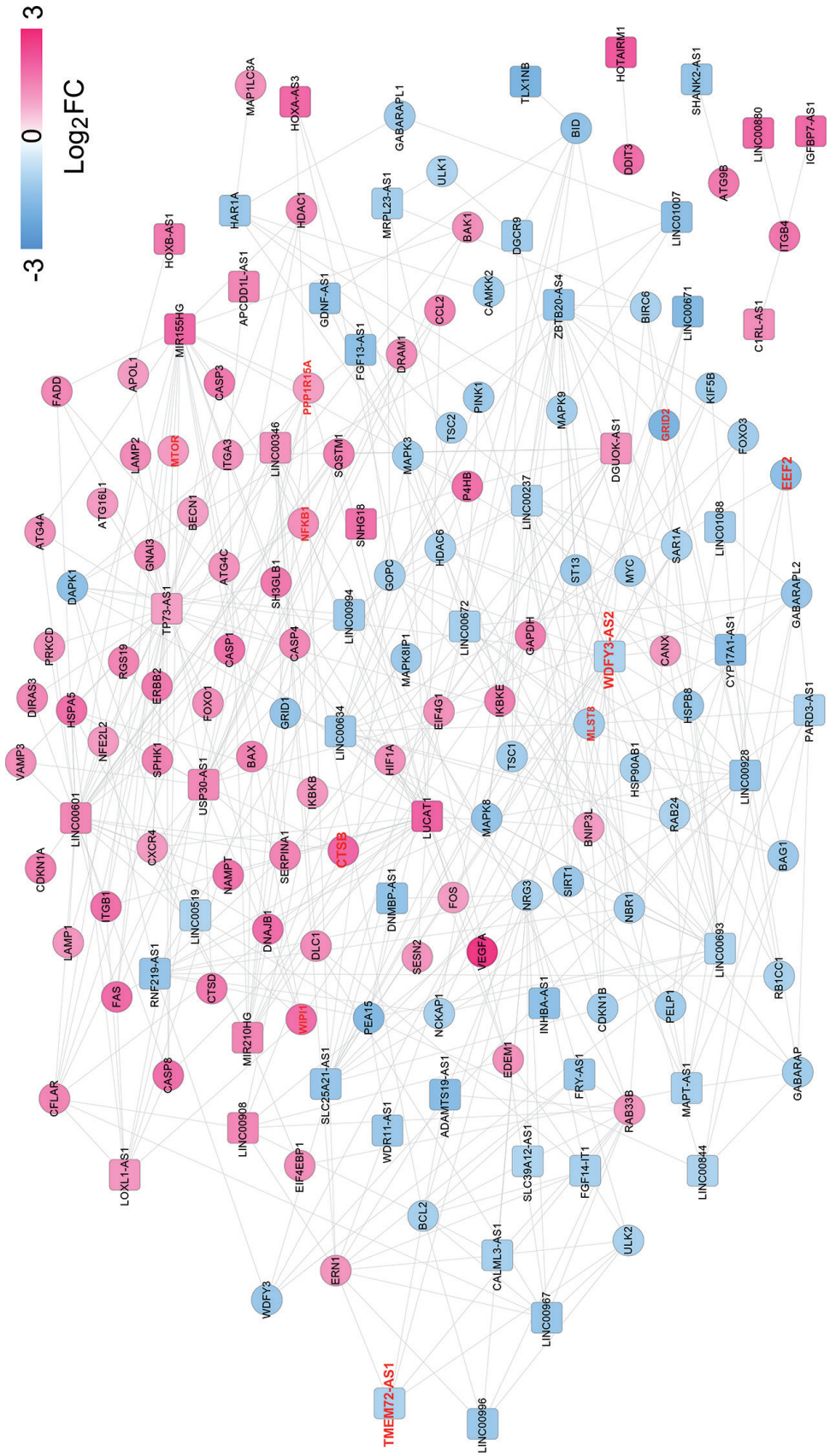

Figure 2. Identification of autophagy-related differentially expressed lncRNAs based on their co-expression with differentially expressed mRNAs. Red, high expression; blue, low expression. Square, lncRNAs; circle, mRNAs. Genes with bold, red color were 10 crucial autophagy-related genes.

Table 1. Function enrichment results

Term	*p*-value	FDR	Genes
Biology Process			
GO:0006914~autophagy	1.53E−22	2.54E−19	GABARAPL2, GABARAPL1, BECN1, ITGB4, RGS19, FOXO1, SESN2, WIPI1, GABARAP, RAB33B, LAMP1, ATG4C, SQSTM1, SH3GLB1, ULK2, ATG4A, RB1CC1, RAB24, CTSD, MTOR, DRAM1
GO:0016236~macroautophagy	2.42E−17	4.01E−14	GABARAPL2, GABARAPL1, BECN1, PINK1, WIPI1, GABARAP, MAP1LC3A, SQSTM1, ULK1, NBR1, RB1CC1, MTOR, MLST8, ATG16L1, HDAC6
GO:0006915~apoptotic process	5.89E−15	9.75E−12	DLC1, FOXO1, NFKB1, PEA15, CASP3, CASP4, BAG1, SH3GLB1, SQSTM1, CXCR4, BCL2, CASP8, FAS, CASP1, CFLAR, BECN1, BIRC6, FADD, PRKCD, DDIT3, DAPK1, NCKAP1, BAX, MAPK3, PPP1R15A, DRAM1
GO:0000422~mitophagy	5.82E−13	9.64E−10	GABARAPL2, ATG9B, GABARAPL1, MAP1LC3A, ATG4C, SQSTM1, ATG4A, RB1CC1, PINK1, WIPI1
GO:0000045~autophagosome assembly	2.80E−12	4.64E−09	GABARAPL2, ATG9B, GABARAPL1, MAP1LC3A, ATG4C, BECN1, ATG4A, RB1CC1, ATG16L1, WIPI1
GO:0043066~negative regulation of apoptotic process	4.71E−12	7.80E−09	CFLAR, BECN1, SPHK1, BIRC6, FOXO1, NFKB1, SIRT1, CASP3, CDKN1A, CDKN1B, BAG1, HDAC1, SQSTM1, BCL2, VEGFA, BNIP3L, MAPK8, HSPA5, FAS, IKBKB, MYC
GO:0071456~cellular response to hypoxia	3.87E−10	6.42E−07	P4HB, EIF4EBP1, HIF1A, BCL2, VEGFA, BNIP3L, PINK1, FOXO3, MTOR, NFE2L2, SIRT1
GO:0016239~positive regulation of macroautophagy	4.52E−09	7.49E−06	HIF1A, ULK1, SQSTM1, BNIP3L, PINK1, SESN2, SIRT1
GO:0097192~extrinsic apoptotic signaling pathway in absence of ligand	5.70E−08	9.44E−05	BAK1, CASP3, BAX, BCL2, FADD, FAS, FOXO3
GO:0042981~regulation of apoptotic process	8.40E−08	1.39E−04	BID, CFLAR, PEA15, CASP4, BAX, CASP8, BNIP3L, FADD, FAS, CTSB, CASP1, DAPK1
GO:0008625~extrinsic apoptotic signaling pathway via death domain receptors	1.15E−07	1.90E−04	BID, BAX, BCL2, FADD, FAS, GABARAP, DAPK1
GO:0006468~protein phosphorylation	1.34E−07	2.21E−04	CCL2, ERBB2, BIRC6, PINK1, PRKCD, CAMKK2, DAPK1, IKBKE, SQSTM1, ULK1, MAPK3, ERN1, MAPK9, MAPK8, MTOR, IKBKB
GO:0007050~cell cycle arrest	2.24E−07	3.72E−04	CDKN1A, CDKN1B, TSC1, TSC2, ERN1, MLST8, MTOR, PPP1R15A, MYC, DDIT3
GO:0071260~cellular response to mechanical stimulus	2.74E−07	4.54E−04	BAK1, MAPK3, CASP8, NFKB1, MAPK8, FADD, FAS, CASP1
GO:1900034~regulation of cellular response to heat	4.01E−07	6.63E−04	HSP90AB1, BAG1, HSPB8, MAPK3, MLST8, DNAJB1, MTOR, SIRT1
GO:0006995~cellular response to nitrogen starvation	9.51E−07	1.58E−03	GABARAPL2, GABARAPL1, MAP1LC3A, BECN1, RB1CC1
GO:0043065~positive regulation of apoptotic process	2.52E−06	4.17E−03	BID, BAK1, SQSTM1, BAX, BNIP3L, FOXO1, MAPK8, FADD, FAS, FOXO3, SIRT1, ITGB1
GO:0097190~apoptotic signaling pathway	5.04E−06	8.35E−03	BAK1, CASP3, BAX, CASP8, FADD, FAS, DAPK1
GO:0001934~positive regulation of protein phosphorylation	1.39E−05	2.30E−02	SQSTM1, RB1CC1, ERBB2, MAPK3, VEGFA, PINK1, MTOR, SIRT1
GO:0010506~regulation of autophagy	1.40E−05	2.33E−02	ULK1, ULK2, CASP1, DRAM1, DAPK1, HDAC6
GO:0009636~response to toxic substance	1.44E−05	2.38E−02	FOS, CDKN1A, BAX, BCL2, MAPK3, FAS, HDAC6
GO:0050821~protein stabilization	2.16E−05	3.58E−02	HSP90AB1, LAMP1, LAMP2, CDKN1A, TSC1, PINK1, PRKCD, GAPDH
GO:0042149~cellular response to glucose starvation	2.93E−05	4.85E−02	BECN1, SH3GLB1, BCL2, HSPA5, NFE2L2

Table 1. Function enrichment results (continued)

Term	*p*-value	FDR	Genes
KEGG Pathway			
hsa05200:Pathways in cancer	4.22E−14	5.09E−11	BID, HSP90AB1, GNAI3, ERBB2, FOXO1, NFKB1, ITGB1, FOS, CASP3, CXCR4, BCL2, CASP8, FAS, MYC, ITGA3, FADD, DAPK1, CDKN1A, CDKN1B, HIF1A, HDAC1, BAX, VEGFA, MAPK3, MAPK9, MAPK8, MTOR, IKBKB
hsa04141:Protein processing in endoplasmic reticulum	1.30E−10	1.57E−07	HSP90AB1, P4HB, CANX, EDEM1, DDIT3, BAK1, BAG1, BAX, BCL2, ERN1, MAPK9, MAPK8, HSPA5, NFE2L2, DNAJB1, PPP1R15A, SAR1A
hsa05161:Hepatitis B	1.48E−10	1.79E−07	NFKB1, FADD, IKBKE, FOS, CDKN1A, CASP3, CDKN1B, BAX, BCL2, CASP8, MAPK3, MAPK9, MAPK8, FAS, IKBKB, MYC
hsa04140:Regulation of autophagy	3.22E−10	3.89E−07	GABARAPL2, GABARAPL1, ATG4C, BECN1, ULK1, ULK2, ATG4A, ATG16L1, GABARAP
hsa05142:Chagas disease (American trypanosomiasis)	4.10E−08	4.95E−05	CFLAR, FOS, GNAI3, CCL2, MAPK3, CASP8, MAPK9, NFKB1, MAPK8, FADD, FAS, IKBKB
hsa04210:Apoptosis	4.68E−08	5.65E−05	BID, CFLAR, CASP3, BAX, BCL2, CASP8, NFKB1, FADD, FAS, IKBKB
hsa04668:TNF signaling pathway	5.53E−08	6.67E−05	CFLAR, FOS, CASP3, CCL2, MAPK3, CASP8, MAPK9, NFKB1, MAPK8, FADD, FAS, IKBKB
hsa05152:Tuberculosis	1.78E−07	2.14E−04	BID, SPHK1, FADD, NFKB1, LAMP1, CASP3, LAMP2, BAX, BCL2, CASP8, MAPK3, CTSD, MAPK9, MAPK8
hsa04066:HIF−1 signaling pathway	2.05E−07	2.48E−04	EIF4EBP1, CDKN1A, CDKN1B, HIF1A, BCL2, ERBB2, MAPK3, VEGFA, NFKB1, MTOR, GAPDH
hsa04621:NOD−like receptor signaling pathway	3.11E−07	3.76E−04	HSP90AB1, CCL2, MAPK3, CASP8, MAPK9, NFKB1, MAPK8, IKBKB, CASP1
hsa04150:mTOR signaling pathway	4.12E−07	4.97E−04	EIF4EBP1, TSC1, ULK1, ULK2, TSC2, MAPK3, MLST8, MTOR, IKBKB
hsa04068:FoxO signaling pathway	5.62E−07	6.79E−04	GABARAPL2, GABARAPL1, CDKN1A, CDKN1B, MAPK3, FOXO1, MAPK9, MAPK8, FOXO3, IKBKB, SIRT1, GABARAP
hsa04151:PI3K−Akt signaling pathway	6.37E−07	7.69E−04	HSP90AB1, ITGB4, NFKB1, ITGA3, FOXO3, ITGB1, EIF4EBP1, CDKN1A, CDKN1B, TSC1, BCL2, VEGFA, MAPK3, TSC2, MTOR, MLST8, IKBKB, MYC
hsa04012:ErbB signaling pathway	9.24E−07	1.12E−03	EIF4EBP1, CDKN1A, CDKN1B, NRG3, ERBB2, MAPK3, MAPK9, MAPK8, MTOR, MYC
hsa05215:Prostate cancer	1.02E−06	1.23E−03	HSP90AB1, CDKN1A, CDKN1B, BCL2, ERBB2, MAPK3, FOXO1, NFKB1, MTOR, IKBKB
hsa05133:Pertussis	3.06E−06	3.70E−03	FOS, CASP3, GNAI3, MAPK3, MAPK9, NFKB1, MAPK8, CASP1, ITGB1
hsa05145:Toxoplasmosis	6.66E−06	8.04E−03	CASP3, GNAI3, BCL2, MAPK3, CASP8, MAPK9, NFKB1, MAPK8, IKBKB, ITGB1
hsa05210:Colorectal cancer	8.99E−06	1.09E−02	FOS, CASP3, BAX, BCL2, MAPK3, MAPK9, MAPK8, MYC
hsa04932:Non−alcoholic fatty liver disease (NAFLD)	1.32E−05	1.60E−02	BID, CASP3, BAX, CASP8, ERN1, MAPK9, NFKB1, MAPK8, FAS, IKBKB, DDIT3
hsa04071:Sphingolipid signaling pathway	1.36E−05	1.64E−02	BID, GNAI3, BAX, BCL2, MAPK3, SPHK1, MAPK9, CTSD, NFKB1, MAPK8
hsa04115:p53 signaling pathway	1.51E−05	1.83E−02	BID, CDKN1A, CASP3, BAX, TSC2, CASP8, FAS, SESN2
hsa05231:Choline metabolism in cancer	2.84E−05	3.43E−02	FOS, EIF4EBP1, HIF1A, TSC1, TSC2, MAPK3, MAPK9, MAPK8, MTOR
hsa04620:Toll−like receptor signaling pathway	4.03E−05	4.87E−02	IKBKE, FOS, MAPK3, CASP8, MAPK9, NFKB1, MAPK8, FADD, IKBKB

GO, Gene Ontology; KEGG, Kyoto Encyclopedia of Genes and Genomes.

95% confidence interval (CI) = 2.092–3.187, p = 2.00e−16] (Fig. 5A). ROC curve analysis further indicated this risk score had an excellent predictive ability for poor prognosis, with the AUC of 0.840 (Fig. 5C). TCGA dataset was used to further validate the predictive power of risk score identified in CGGA dataset. In line with the results derived from the CGGA dataset, patients with high risk scores were also seen to possess a shorter OS than those with low risk scores (HR = 1.630, 95%CI = 1.266–2.098, p = 1.344e−04) (Fig. 5B). The AUC was 0.744 (Fig. 5D).

Univariate and multivariate Cox regression analyses were then performed to evaluate the prognostic independence of the autophagy signature and various clinicopathologic parameters. Consequentially, age (Fig. 6A), recurrence status

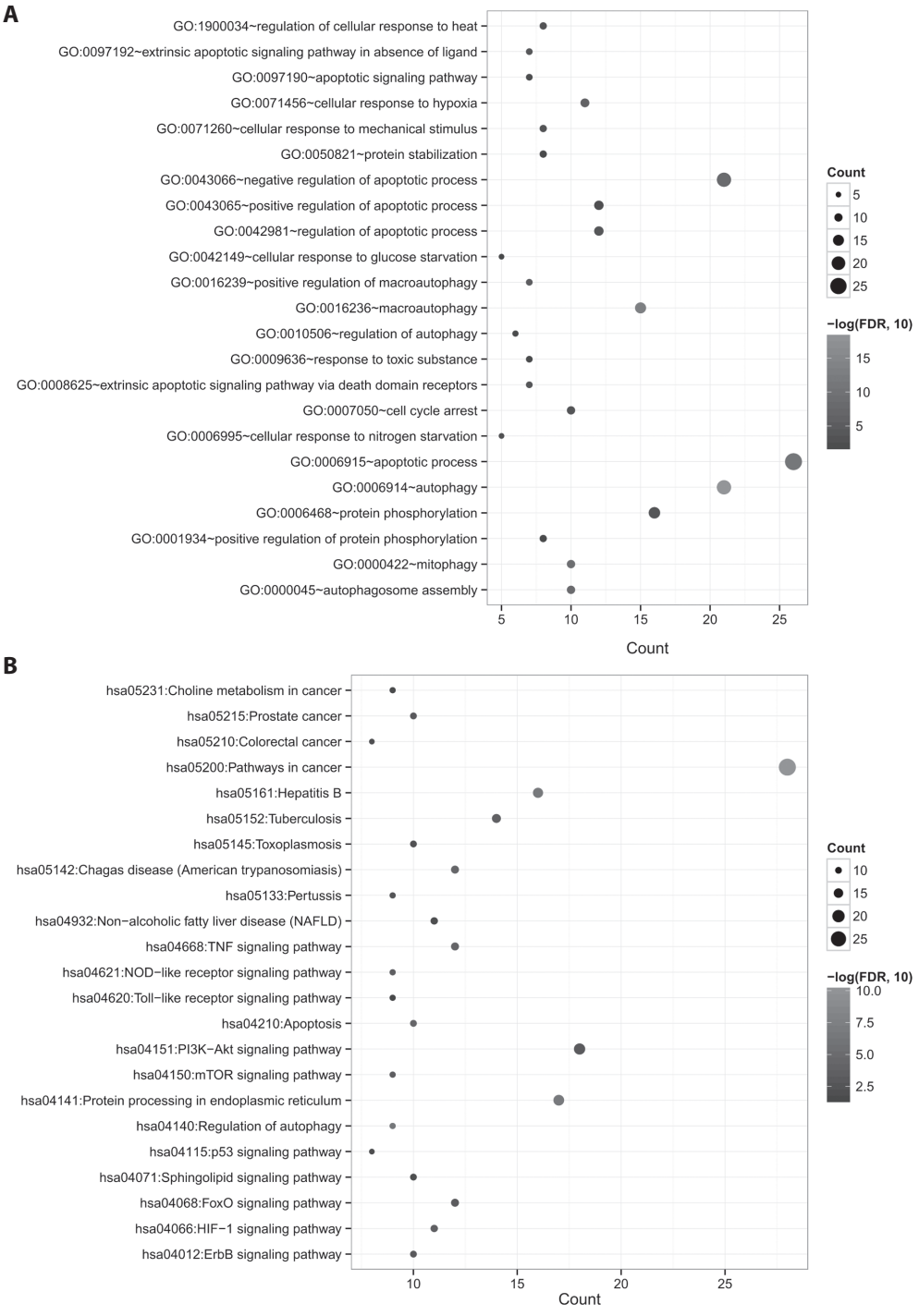

Figure 3. Function enrichment analysis for genes in the co-expression network by DAVID. **A.** Gene ontology (GO) biological process terms. **B.** Kyoto Encyclopedia of Genes and Genomes (KEGG).

(Fig. 6D), radio status, chemo status, IDH mutation status (Fig. 6G) and risk score status were found to be associated with OS in univariate analysis, while only age, recurrence status, IDH mutation status and risk score status were identified as independent prognostic factors in multivariate analysis (Table 3). Furthermore, stratification analysis revealed that the risk score also could divide patients with the same age (≥ 45 years, p = 1.115e−09, Fig. 6B; < 45 years, p = 5.202e−09, Fig. 6C), recurrence status (without recurrence, p = 1.11e−16, Fig. 6E; recurrence, p = 2.532e−04, Fig. 6F) and IDH status (without mutation, p = 9.323e−03, Fig. 6H; with mutation, p = 3.675e−07, Fig. 6I) into the high-risk (shorter OS) and low-risk (longer OS), suggesting the prognostic performance of the risk score was better than those clinical factors. This conclusion was also validated by time-dependent ROC curve (risk score: AUC = 0.84 *vs*. 0.608, age; 0.599, recurrence status; 0.672, IDH mutation status) and C-index (risk score: 0.738 *vs*. 0.592, age; 0.596, recurrence status; 0.661, IDH mutation status) (Fig. 7A; Table 4). Thus, the risk score was suggested to be incorporated into the clinical factors for prognosis prediction in clinic, based on which a nomogram was built (Fig. 7B). The calibration curves showed that the predicted possibility of OS was similar to the actual OS (Fig. 7C). The AUC (0.879) and C-index (0.773) of nomogram was also higher than age, recurrence status, IDH status and risk score (Fig. 7A).

Discussion

In the present study, we, for the first time, identified autophagy-related DERs between GBM and LGG and used them to construct the diagnostic and prognostic signature for glioma patients. As a result, 10 signature genes (TMEM72-AS1, WDFY3-AS2, CTSB, EEF2, GRID2, MLST8, MTOR, NFKB1, PPP1R15A and WIPI1) were obtained. This signature could obviously distinguish GBM from LGG, with the accuracy of 0.891 using CGGA dataset and 0.790 using TCGA dataset. Its related risk score effectively screened the patients at an increased risk of developing GBM (49.7% *vs*. 21.3%, p < 0.001) or ones (GBM and possibly progress to GBM) with poor OS. The prognostic accuracy was 0.840 and 0.744 using CGGA and TCGA dataset, respectively. These results were comparable to other risk classification systems established by the lipid metabolism (Wu et al. 2019), pseudogenes (Wang et al. 2019a), necrosis (Wang and Ma 2019) or module (Wang et al. 2019b) related genes that were differentially expressed between GBM and LGG. Furthermore, previous studies indicated mRNA signature outperformed the lncRNA-based signature (Gong et al. 2020), while combined with lncRNAs (Liu Q 2020; Wang 2020a) added the power in predicting prognosis. Thus, we screened the combined lncRNA-mRNA signature and

Table 2. Identified signature genes

Symbol	Type	Expression		Logit regression				Univariate Cox regression			Multivariate Cox regression			
		Log_2FC	FDR	Estimate	SE	z-value	p-value	Coef.	HR	p-value	Coef.	p-value	HR	95%CI
TMEM72−AS1	lncRNA	−1.05	1.11E−18	4.4549	1.0097	4.412	1.02E−05	−2.47	0.0848	3.70E−10	−2.419	1.60E−04	0.08902	0.02536−0.3125
WDFY3−AS2	lncRNA	−1.02	8.85E−25	0.2569	0.0757	3.395	6.86E−04	−0.132	0.876	1.50E−09	−0.1293	2.45E−02	0.87869	0.78502−0.9835
CTSB	mRNA	1.88	8.02E−12	0.0010	0.0005	2.001	4.54E−02	0.000478	1	1.60E−06	−0.0009808	4.00E−02	0.99902	0.99808−0.9999
EEF2	mRNA	−1.51	7.53E−09	0.0004	0.0002	2.694	7.06E−03	−0.000386	1	3.30E−08	−0.0002811	4.68E−02	0.99972	0.99944−0.9999
GRID2	mRNA	−1.84	2.59E−10	0.0926	0.0465	1.994	4.61E−02	−0.0822	0.921	7.00E−05	−0.1031	4.02E−03	0.90205	0.84087−0.9677
MLST8	mRNA	−1.18	3.06E−05	0.0085	0.0039	2.167	3.02E−02	−0.00685	0.993	2.20E−07	−0.01185	2.60E−02	0.98822	0.97797−0.9986
MTOR	mRNA	1.07	7.65E−03	−0.0593	0.0225	−2.637	8.37E−03	0.0453	1.05	2.50E−09	0.04575	4.64E−02	1.04682	1.00074−1.095
NFKB1	mRNA	1.25	1.45E−06	0.1318	0.0609	2.164	3.05E−02	0.106	1.11	2.90E−15	−0.1039	3.39E−02	0.90134	0.81886−0.9921
PPP1R15A	mRNA	1.02	2.66E−20	−0.0279	0.0110	−2.539	1.11E−02	0.013	1.01	2.10E−14	−0.01613	2.62E−02	0.984	0.97011−0.9981
WIPI1	mRNA	1.74	1.27E−19	−0.1029	0.0322	−3.197	1.39E−03	0.057	1.06	0.00E+00	0.04084	3.60E−02	1.04168	1.00267−1.0822

FDR, false discovery rate; SE, standard error; Coef, coefficient; HR, hazard ratio; CI, confidence interval.

compared the predictive performance of three classifiers. As expected, the AUC (0.84 *vs.* 0.809; 0.685) and C-index (0.738 *vs.* 0.696; 0.639) of lncRNA-mRNA signature were the highest compared with mRNA and lncRNA alone. In line with other signatures reported in glioma patients, the risk score generated in our study was also independent of other clinicopathologic factors (Wang et al. 2019b; Wang et al. 2019c; Wang et al. 2020a) and even superior to the variables that were also independent in multivariate analysis [(risk score: AUC = 0.84 *vs.* 0.608, age; 0.599, recurrence status; 0.672, IDH mutation status) and C-index (risk score: 0.738 *vs.* 0.592, age; 0.596, recurrence status; 0.661, IDH mutation status)] (Wang et al. 2021). These findings suggested our new risk score may be a promising biomarker for GBM diagnosis and prognosis. In order to obtain better predictive effects in clinic, recent studies recommended to creating a nomogram that integrated the molecular signature with clinical indicators (Wang et al. 2019a, 2019b; Wang et al. 2019c; Wang et al. 2020c). Similarly, a nomogram based on the risk signature, age, recurrence status and IDH mutation status was established in the training cohort. The AUC and C-index reached 0.879 and 0.773, respectively. Calibration curves showed that there were good agreements between the predicted and observed 3- and 5-year OS. Accordingly, this nomogram may be a clinically simple-to-use tool for prognostic prediction in glioma patients.

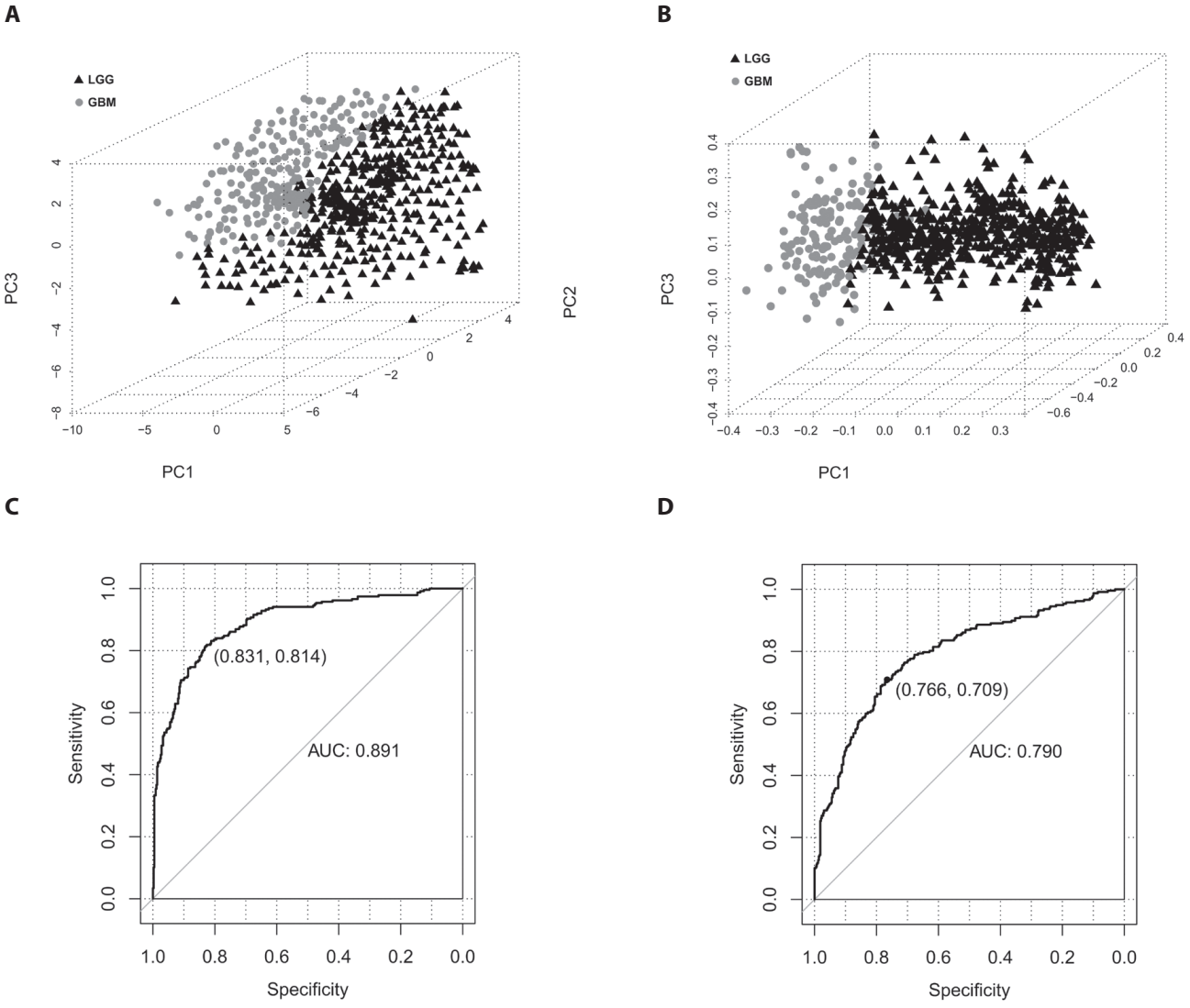

Figure 4. Logit regression model to identify the feature genes to distinguish GBM from LGG. Scatter plot for CGGA (**A**) and TCGA (**B**) dataset. Red, GBM samples; black, LGG samples; PC1, PC2, PC3, the first, second, third principal component. Receiver operator characteristic (ROC) curve for CGGA (**C**) and TCGA (**D**) dataset. AUC, area under the ROC curve. For more abbreviations, see Fig. 1.

Table 3. Univariate and multivariate analyses of overall survival

Variables	CGGA (n = 668)	Univariate analysis			Multivariate analysis		
		HR	95%CI	p–value	HR	95%CI	p–value
Age (years, mean ± SD)	43.36 ± 12.36	1.027	1.018–1.035	1.55E–09	1.009	1.001–1.018	4.83E–02
Gender (Male/Female)	380/288	1.012	0.826–1.241	9.07E–01	–	–	–
Recurrence (Yes/No/–)	259/409	2.089	1.702–2.564	1.74E–12	2.266	1.813–2.833	6.74E–13
Radio status (Yes/No/–)	505/110/53	1.431	1.058–1.935	1.53E–02	1.019	0.725–1.430	9.16E–01
Chemo status (Yes/No/–)	454/149/65	1.506	1.154–1.966	1.70E–03	0.741	0.542–1.015	6.17E–02
IDH mutation status (Wildtype/Mutate/–)	277/343/48	0.309	0.249–0.382	2.00E–16	0.526	0.407–0.679	9.21E–07
Risk score status (High/Low)	380/288	2.582	2.092–3.187	2.00E–16	1.707	1.347–2.165	1.01E–05

HR, hazard ratio; CI, confidence interval; SD, standard deviation; IDH, isocitrate dehydrogenase; CGGA, The Chinese Glioma Genome Atlas.

All these autophagy-related signature mRNAs (CTSB, EEF2, GRID2, MLST8, MTOR, NFKB1, PPP1R15A and WIPI1) had been demonstrated to be associated with the progression of glioma or other cancers. CTSB, which encodes lysosomal cysteine proteinase protein, was reported to be upregulated in GBM cancer cells and stem cell niches (Pucer et al. 2010; Jennewein et al. 2016; Breznik et al. 2018). Overexpression of CTSB decreased chemotherapeutic temozolomide drug-induced glioma cell death and promoted the mesenchymal transition (Ho et al. 2019); while knockdown of CTSB caused cell cycle arrested in G0/G1 phases and enhanced radiosensitivity (Zhang et al. 2018). Elevated CTSB may, like cathepsin L, contributed to radio-resistance in human glioma cells by activation of its downstream NF-κB (Yang et al. 2015). The expression of NF-κB1 was revealed to be increased with the increasing degree of malignancy in glioma (Yang et al. 2014). PI3K/Akt/mTOR was a highly activated signaling pathway to induce autophagy for GBM cells (Li et al. 2016). When the PI3K/Akt/mTOR pathway was blocked by using their corresponding inhibitors, the migration and invasion of GBM U87 cells were shown to be suppressed (Huang et al. 2018). MLST8 combined with mTOR, Rictor, mSin1 and Protor to form the autophagy inhibitor rapamycin-insensitive complex (mTORC2). Increased mTORC2 activity promoted glioma growth and cell motility (Masri et al. 2007). Disruption of the scaffolding function of MLST8 inhibited mTORC2 assembly and its-dependent tumor growth (Hwang et al. 2019). EEF-2 kinase was involved in autophagy by acting as a downstream member of the mTOR signaling pathway (Wu et al. 2009). RNA interference analysis showed silencing of EEF-2 markedly inhibited autophagy and decreased the viability, migration and invasion ability of GBM cells (Wu et al. 2009; Zhang et al. 2011; Liu et al. 2013). PPP1R15A (also known as GADD34) was found to be expressed following DNA damage, a major inducer in hypoxia to activate autophagy (Ito et al. 2015). Hypoxia was reported to upregulate PPP1R15A in glioma cells compared with control (Minchenko et al. 2016). Inhibition of PPP1R15A greatly suppressed anaplastic thyroid carcinoma cell growth (Cao et al. 2019) and potentiated tumor necrosis factor-related apoptosis-inducing ligand (TRAIL)-induced apoptosis of hepatocellular carcinoma cells (Song et al. 2019). Elevated expression of PPP1R15A was associated with poor clinical prognosis (Cao et al. 2019). WIPI1 was suggested to serve as an autophagy biomarker protein (Tsuyuki et al. 2014). It

Table 4. The performance of the nomogram assessed by different classifiers

Model	AUC	C-index	p-value	Specificity	Sensitivity
Age model	0.608	0.592	3.513E–09	0.624	0.584
Recurrence model	0.599	0.596	8.549E–14	0.662	0.537
IDH mutation model	0.672	0.661	0	0.755	0.588
Clinical model	0.671	0.731	0	0.685	0.66
LncRNAs alone	0.685	0.639	0	0.525	0.793
mRNAs alone	0.809	0.696	0	0.65	0.834
multi-RNAs based model	0.84	0.738	0	0.743	0.795
multi-RNAs combined clinical model	0.879	0.773	0	0.918	0.685

AUC, area under the curve of receiver operating characteristic curve; C-index, concordance index; IDH, isocitrate dehydrogenase.

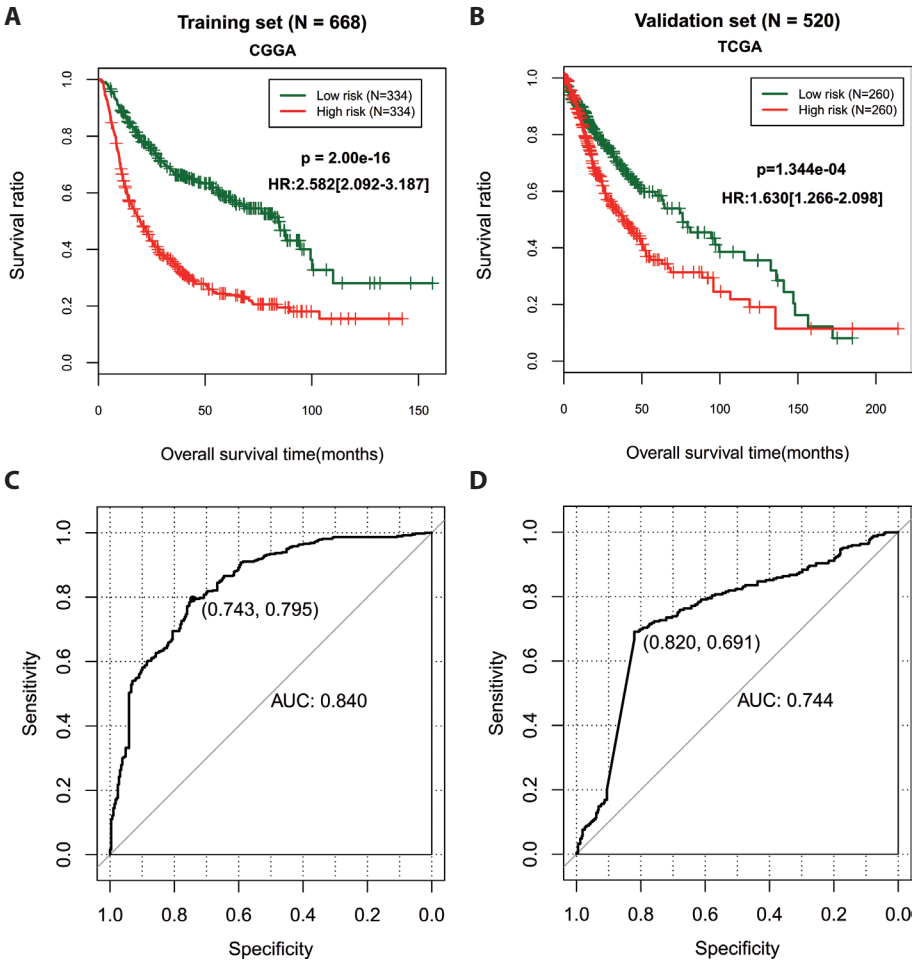

Figure 5. The prognostic performance of the autophagy-related risk score model for glioma patients. Kaplan-Meier survival curve analysis to show the overall survival difference of patients with high risk score and low-risk score in the CGGA (**A**) and TCGA (**B**) dataset. Receiver operator characteristic (ROC) to demonstrate the prognostic power of risk score for the overall survival of patients in the CGGA (**C**) and TCGA (**D**) dataset. HR, hazard ratio; AUC, area under the ROC curve. For more abbreviations, see Fig. 1.

was upregulated in clinical hepatocellular carcinoma (Shi et al. 2016) and melanoma samples (D'Arcangelo and Giampietri 2018). Wang et al. (2021) identified patients with high expression level of GRID2 may have a better prognosis than those with low expression levels. In line with these findings, we also found MTOR, NFKB1, PPP1R15A, WIPI1 and CTSB were higher expressed, while GRID2 was lower expressed in GBM compared with LGG. These genes were enriched in autophagy, apoptosis and cell cycle biological processes or pathways. The expressions of EEF2 and MLST8 were not upregulated as expected, which may be the possible difference between wet and dry experiments or their dual functions.

There were studies to explore lncRNAs that play important roles in glioma by influencing autophagy and its related genes. Luan et al. (2019) used the CGAA dataset to identify 10 autophagy-associated lncRNAs with prognostic value (PCBP1-AS1, TP53TG1, DHRS4-AS1, ZNF674-AS1, GABPB1-AS1, DDX11-AS1, SBF2-AS1, MIR4453HG, MAPKAPK5-AS1 and COX10-AS1). Their established risk score could distinguish the OS between the low-risk group and high-risk group, which was also validated using the TCGA dataset. LncRNA MALAT1 activated autophagy and promoted cell proliferation of glioma cells by upregulating autophagy genes STMN1, RAB5A and ATG4D (Fu et al. 2017), while knockdown of MALAT1 inhibited cell migration and invasion of glioma cells by suppressing autophagy through regulation of autophagy gene GOLM1 (Ma et al. 2020). Elevated lncRNA AC023115.3 and growth arrest-specific 5 (GAS5) in human GBM cells were demonstrated to promote cisplatin-induced apoptosis by inhibiting autophagy (Ma et al. 2017; Huo and Chen 2019). However, autophagy-related lncRNAs remain rarely reported. In our study, we identified TMEM72-AS1 and WDFY3-AS2 may be important biomarkers for glioma patients to separate GBM from LGG and predict their prognosis. WDFY3-AS2 was previously reported in the study of Wu et al. (2018) who found WDFY3-AS2 was one downregulated lncRNA in GBM compared with LGG and patients with high WDFY3-AS2 expression had longer OS than the low expression ones. These conclusions were also demonstrated in our study. However, compared with

individual WDFY3-AS2 (Wu et al. 2018), our combined signature (including WDFY3-AS2 and other genes) may be more effective for clinical application of prognosis prediction (AUC = 0.840 *vs.* 0.796). More importantly, the study of Wu et al. (2018) did not provide the specific downstream target genes to explain the functions of WDFY3-AS2. Our study, for the first time, speculated WDFY3-AS2 may function by co-expressing with SIRT1, FoxO3a, TSC1 and HIF1A. These co-expressed genes have been demonstrated to act as suppressor genes for the

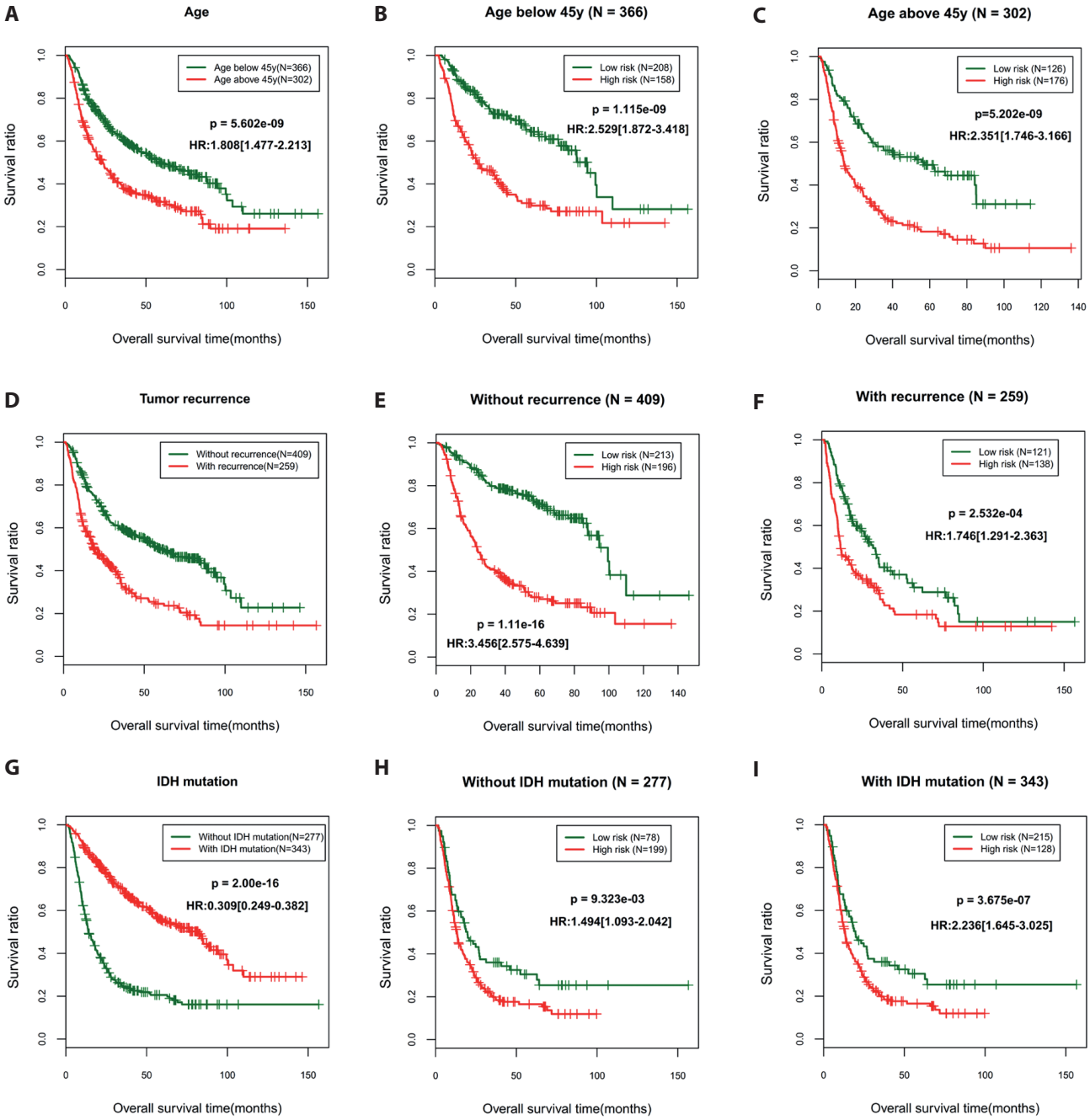

Figure 6. Risk stratification model based on age, recurrence and IDH mutation for glioma patients. The association of age (**A**), recurrence (**D**) and IDH mutation (**G**) with overall survival. The prognosis of patients in the age range (below 45 years (**B**) and above 45 years (**C**)) according to the risk score. The prognosis of patients in the different recurrence status according to the risk score (**E** and **F**). The prognosis of patients without (**H**) and with (**I**) IDH mutation status according to the risk score. HR, hazard ratio; y, year; IDH, isocitrate dehydrogenase.

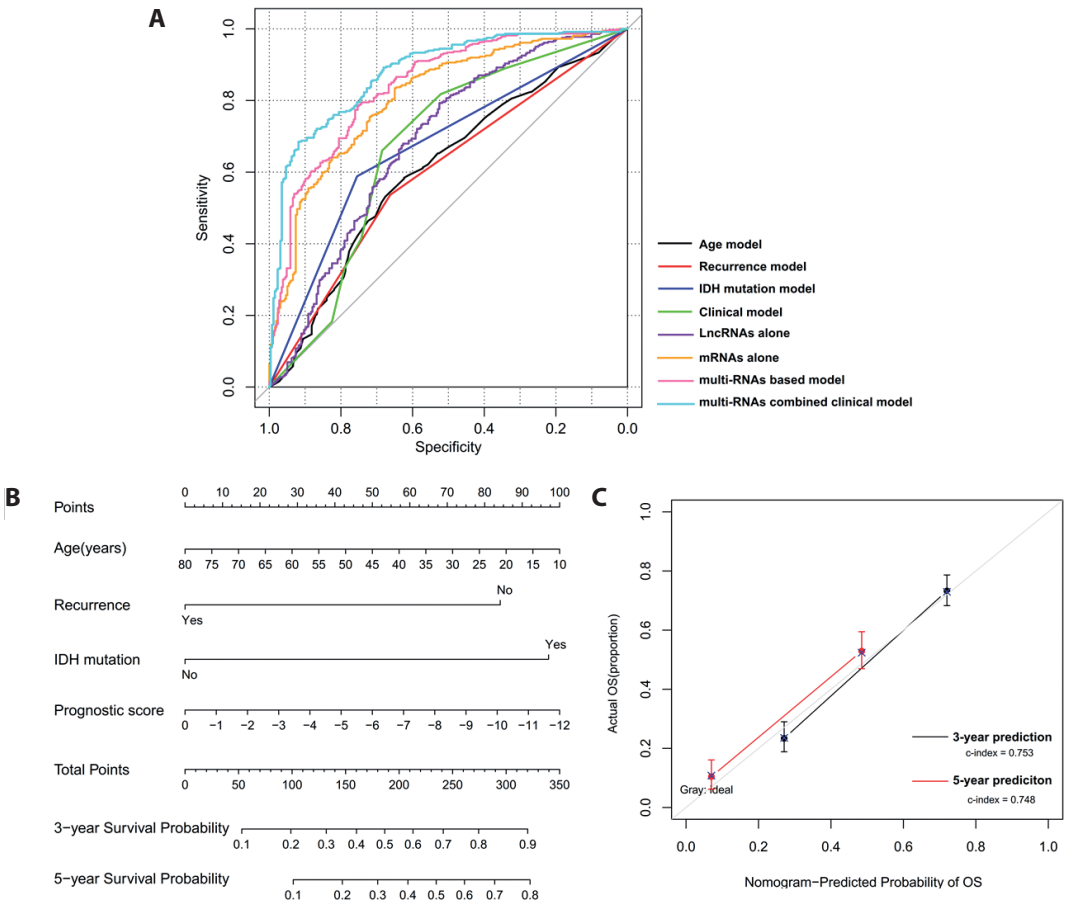

Figure 7. A prognostic nomogram to predict the survival probability of patients with glioma. **A.** Receiver operator characteristic curve to demonstrate the superiority of risk score for prognosis prediction to other clinical factors. **B.** A prognostic nomogram. **C.** Calibration curves.

progression of GBM or other cancers. It was reported that SIRT1 hindered autophagy and GBM growth by mediating the deacetylation of p21-activated kinase 1 (PAK1) at K420 and suppressing the PAK1-ATG5 (autophagy related 5) pathway (Feng et al. 2021). FoxO3a was found to be a negative regulator of autophagy in multiple cancer cells (Zhu et al. 2014). Increased FOXO3a inhibited autophagy and stimulated transcription of the pro-apoptotic BBC3/PUMA gene to cause apoptosis sensitization, thus reducing tumor burden (Fitzwalter et al. 2018). SIRT1 exerted inhibitory activities on chemoresistance and cancer stemness of gastric cancer by initiating the transcription of FOXO3 (An et al. 2020). TSC1, a negative regulator of mTOR signaling, was downregulated in high-grade serous ovarian carcinoma compared with normal fimbria and low stage patients. Ectopic expression of TSC1 could block cell proliferation, migration and autophagy (Wang et al. 2017). Hypoxia induced autophagy in glioma LN229 cells through upregulating the expression of HIF1A expression. Knockout of HIF1A inhibited cell motility and chemosensitivity (Hu et al. 2012; Huang et al. 2019). Furthermore, it was observed that the concentrations of betaine, phosphocholine and choline were lowed in HIF1B-deficient hepatoma compared with wide type (Griffiths et al. 2002); while these choline metabolism products were elevated in glioma (Gillies et al. 1994) and targeted drugs may treat GBM by decreasing phosphocholine and choline kinase α (Venkatesh et al. 2012), suggesting HIF1A may also be involved in the glioma progression by influencing choline metabolism. In line with these studies, SIRT1, FoxO3a and TSC1 were also shown to be downregulated, while HIF1A was upregulated in GBM compared with LGG. These genes were not only autophagy-related, but also enriched in various pathways [hsa04066:HIF-1 signaling pathway (HIF1A), hsa04068:FoxO signaling pathway (FOXO3, SIRT1), hsa04150:mTOR signaling pathway (TSC1) and hsa05231:Choline metabolism in cancer (TSC1, HIF1A)]. The roles of TMEM72-AS1 had not been illustrated for any diseases. Our study, for the first time, predicted it may be one crucial lncRNA for malignant progression of glioma

by regulating autophagy-related ULK2. The protein expression level of ULK2 was observed to be significantly lower in NSCLC cases (Cheng et al. 2019) and glioma (Shukla et al. 2014) compared with control. Overexpression of ULK2 significantly inhibited the proliferation of A549 and H460 cells and improved the chemosensitivity to cisplatin and etoposide. Overexpression of ULK2 also suppressed tumor volume *in vivo* (Cheng et al. 2019). Our expression level of ULK2 in GBM was consistent with the study of Cheng et al. (2019) and Shukla et al. (2014). However, unfortunately, several studies suggested ULK2 may also induce autophagy, not inhibit autophagy in cancer (John Shukla et al. 2014; Clotaire et al. 2016; Cheng et al. 2019). This may be, on one hand, attributed to the dual functions of autophagy; on the other hand, may be associated with the response loop (Wang et al. 2018). Thus, the combination treatment of ULK overexpression with autophagy inhibitors may potentially be a more effective therapeutic strategy for GBM.

There were some limitations in this study. First, the proposed signature was established and validated using the public datasets. The newly hospitalized GBM and LGG patients in our hospital should be enrolled to further investigate the performance of the signature. Second, functional experiments should be performed to explore the relationship between our identified lncRNAs and mRNAs (TMEM72-AS1-ULK2, WDFY3-AS2-SIRT1/FoxO3/TSC1) and their associations with progression of glioma.

Conclusion

Our study successfully developed a novel 10-gene signature constituted by 2 lncRNAs and 8 autophagy-related genes. This signature distinguished GBM from LGG and predicted OS in patients with glioma. The established nomogram that integrated the risk score and clinical parameters may be more effective to aid the clinical decision making of personalized treatment.

Acknowledgements. This study was supported by the Science and Technology of Jilin Province (No. 20200201470JC).

Availability of data and materials. All data were collected from CGGA (http://www.cgga.org.cn) and TCGA (https://gdc-portal.nci.nih.gov/) and databases.

Authors' contributions. BW, LW and JWZ conceived and designed the original study. BW and LW analyzed the data and drafted the manuscript. JWZ contributed to the interpretation of data and revised the manuscript. All authors read and approved the final manuscript.

Conflict of interest. The authors declare that they have no competing interests.

References

Almutrafi A, Bashawry Y, AlShakweer W, Al-Harbi M, Altwairgi A, Al-Dandan S (2020): The epidemiology of primary central nervous system tumors at the National Neurologic Institute in Saudi Arabia: A Ten-year single-institution study. J. Cancer Epidemiol. **2020,** 1429615 https://doi.org/10.1155/2020/1429615

An Y, Wang B, Wang X, Dong G, Jia J, Yang Q (2020): SIRT1 inhibits chemoresistance and cancer stemness of gastric cancer by initiating an AMPK/FOXO3 positive feedback loop. Cell Death Dis. **11,** 115 https://doi.org/10.1038/s41419-020-2308-4

Araghi M, Roshandel G, Hasanpour-Heidari S, Fazel A, Sedaghat SM, Pourkhani A, Kazeminejhad V, Miranda-Filho A, Bray F, Arnold M (2020): Incidence of malignant brain and central nervous system tumors in Golestan, Iran, 2004-2013. Arch. Iran Med. **23,** 1-6

Biterge-Sut B (2020): A comprehensive analysis of the angiogenesis-related genes in glioblastoma multiforme vs. brain lower grade glioma. Arq. Neuropsiquiatr. **78,** 34-38 https://doi.org/10.1590/0004-282x20190131

Breznik B, Limbaeck Stokin C, Kos J, Khurshed M, Hira VVV, Bošnjak R, Lah TT, Van Noorden CJF (2018): Cysteine cathepsins B, X and K expression in peri-arteriolar glioblastoma stem cell niches. J. Mol. Histol. **49,** 481-497 https://doi.org/10.1007/s10735-018-9787-y

Cao X, Dang L, Zheng X, Lu Y, Lu Y, Ji R, Zhang T, Ruan X, Zhi J, Hou X, et al. (2019): Targeting super-enhancer-driven oncogenic transcription by CDK7 inhibition in anaplastic thyroid carcinoma. Thyroid **29,** 809-823 https://doi.org/10.1089/thy.2018.0550

Cheng H, Yang ZT, Bai YQ, Cai YF, Zhao JP (2019): Overexpression of Ulk2 inhibits proliferation and enhances chemosensitivity to cisplatin in non-small cell lung cancer. Oncol. Lett. **17,** 79-86 https://doi.org/10.3892/ol.2018.9604

Cj P, Hv E, Vijayakurup V, R Menon G, Nair S, Gopala S (2019): High LC3/beclin expression correlates with poor survival in glioma: a definitive role for autophagy as evidenced by in vitro autophagic flux. Pathol. Oncol. Res. **25,** 137-148 https://doi.org/10.1007/s12253-017-0310-7

D'Arcangelo D, Giampietri C (2018): WIPI1, BAG1, and PEX3 autophagy-related genes are relevant melanoma markers. Oxid. Med. Cell Longev. **2018,** 1471682 https://doi.org/10.1155/2018/1471682

Dennis G, Sherman BT, Hosack DA, Yang J, Gao W, Lane HC, Lempicki RA (2003): DAVID: Database for annotation, visualization, and integrated discovery. Genome Biol. **4,** P3 https://doi.org/10.1186/gb-2003-4-5-p3

Feng X, Zhang H, Meng L, Song H, Zhou Q, Qu C, Zhao P, Li Q, Zou C, Liu X, Zhang Z (2021): Hypoxia-induced acetylation of PAK1 enhances autophagy and promotes brain tumorigenesis via phosphorylating ATG5. Autophagy **17,** 723-742 https://doi.org/10.1080/15548627.2020.1731266

Fitzwalter BE, Towers CG, Sullivan KD, Andrysik Z, Hoh M, Ludwig M, O'Prey J, Ryan KM, Espinosa JM, Morgan MJ, Thorburn A (2018): Autophagy inhibition mediates apoptosis

sensitization in cancer therapy by relieving FOXO3a turnover. Dev. Cell. **44,** 555-565.e553
https://doi.org/10.1016/j.devcel.2018.02.014

Fu Z, Luo W, Wang J, Peng T, Sun G, Shi J, Li Z, Zhang B (2017): Malat1 activates autophagy and promotes cell proliferation by sponging miR-101 and upregulating STMN1, RAB5A and ATG4D expression in glioma. Biochem. Biophys. Res. Commun. **492,** 480-486
https://doi.org/10.1016/j.bbrc.2017.08.070

Gillies RJ, Barry JA, Ross BD (1994): In vitro and in vivo 13C and 31P NMR analyses of phosphocholine metabolism in rat glioma cells. Magn. Reson. Med. **32,** 310-318
https://doi.org/10.1002/mrm.1910320306

Gong Z, Hong F, Wang H, Zhang X, Chen J (2020): An eight-mRNA signature outperforms the lncRNA-based signature in predicting prognosis of patients with glioblastoma. BMC Med. Genet. **21,** 56
https://doi.org/10.1186/s12881-020-0992-7

Griffiths JR, McSheehy PM, Robinson SP, Troy H, Chung YL, Leek RD, Williams KJ, Stratford IJ, Harris AL, Stubbs M (2002): Metabolic changes detected by in vivo magnetic resonance studies of HEPA-1 wild-type tumors and tumors deficient in hypoxia-inducible factor-1beta (HIF-1beta): evidence of an anabolic role for the HIF-1 pathway. Cancer Res. **62,** 688-695

Ho KH, Cheng CH, Chou CM, Chen PH, Liu AJ, Lin CW, Shih CM, Chen KC (2019): miR-140 targeting CTSB signaling suppresses the mesenchymal transition and enhances temozolomide cytotoxicity in glioblastoma multiforme. Pharmacol. Res. **147,** 104390
https://doi.org/10.1016/j.phrs.2019.104390

Hu YL, DeLay M, Jahangiri A, Molinaro AM, Rose SD, Carbonell WS, Aghi MK (2012): Hypoxia-induced autophagy promotes tumor cell survival and adaptation to antiangiogenic treatment in glioblastoma. Cancer Res. **72,** 1773-1783
https://doi.org/10.1158/0008-5472.CAN-11-3831

Huang W, Ding X, Ye H, Wang J, Shao J, Huang T (2018): Hypoxia enhances the migration and invasion of human glioblastoma U87 cells through PI3K/Akt/mTOR/HIF-1α pathway. Neuroreport **29,** 1578-1585
https://doi.org/10.1097/WNR.0000000000001156

Huang S, Qi P, Zhang T, Li F, He X (2019): The HIF-1α/miR-224-3p/ATG5 axis affects cell mobility and chemosensitivity by regulating hypoxia-induced protective autophagy in glioblastoma and astrocytoma. Oncol. Rep. **41,** 1759-1768
https://doi.org/10.3892/or.2018.6929

Huo JF, Chen XB (2019): Long noncoding RNA growth arrest-specific 5 facilitates glioma cell sensitivity to cisplatin by suppressing excessive autophagy in an mTOR-dependent manner. J. Cell Biochem. **120,** 6127-6136
https://doi.org/10.1002/jcb.27900

Hwang Y, Kim LC, Song W, Edwards DN (2019): Disruption of the scaffolding function of mLST8 selectively inhibits mTORC2 assembly and function and suppresses mTORC2-dependent tumor growth in vivo. Cancer Res. **79,** 3178-3184
https://doi.org/10.1158/0008-5472.CAN-18-3658

Ito S, Tanaka Y, Oshino R, Aiba K, Thanasegaran S, Nishio N, Isobe K (2015): GADD34 inhibits activation-induced apoptosis of macrophages through enhancement of autophagy. Sci. Rep. **5,** 8327
https://doi.org/10.1038/srep08327

Jennewein L, Ronellenfitsch MW, Antonietti P, Ilina EI, Jung J, Stadel D, Flohr LM, Zinke J, von Renesse J, Drott U, et al. (2016): Diagnostic and clinical relevance of the autophago-lysosomal network in human gliomas. Oncotarget **7,** 20016-20032
https://doi.org/10.18632/oncotarget.7910

Jiang T, Wu Z (2018): Immunohistochemical assessment of autophagic protein LC3B and p62 levels in glioma patients. Int. J. Clin. Exp. Pathol. **11,** 862-868

John Clotaire DZ, Zhang B, Wei N, Gao R, Zhao F, Wang Y, Lei M, Huang W (2016): MiR-26b inhibits autophagy by targeting ULK2 in prostate cancer cells. Biochem. Biophys. Res. Commun. **472,** 194-200
https://doi.org/10.1016/j.bbrc.2016.02.093

Li X, Wu C, Chen N, Gu H, Yen A, Cao L, Wang E, Wang L (2016): PI3K/Akt/mTOR signaling pathway and targeted therapy for glioblastoma. Oncotarget **7,** 33440-33450
https://doi.org/10.18632/oncotarget.7961

Li X, He S, Ma B (2020): Autophagy and autophagy-related proteins in cancer. Mol. Cancer **19,** 12
https://doi.org/10.1186/s12943-020-1138-4

Liu Q, Wang Z, Kong X, Wang X, Qi Y, Gao R, Fang Y, Wang J (2020): A Novel prognostic signature of mRNA-lncRNA in breast cancer. DNA Cell Biol. **39,** 671-682
https://doi.org/10.1089/dna.2019.5223

Liu XY, Zhang L, Wu J, Zhou L, Ren YJ, Yang WQ, Ming ZJ, Chen B, Wang J, Zhang Y, Yang JM (2013): Inhibition of elongation factor-2 kinase augments the antitumor activity of Temozolomide against glioma. Plos One **8,** e81345
https://doi.org/10.1371/journal.pone.0081345

Luan F, Chen W, Chen M, Yan J, Chen H, Yu H, Liu T, Mo L (2019): An autophagy-related long non-coding RNA signature for glioma. Febs. Open Bio. **9,** 653-667
https://doi.org/10.1002/2211-5463.12601

Ma B, Yuan Z, Zhang L, Lv P, Yang T, Gao J, Pan N, Wu Q, Lou J, Han C, Zhang B (2017): Long non-coding RNA AC023115.3 suppresses chemoresistance of glioblastoma by reducing autophagy. Biochim. Biophys. Acta **1864,** 1393-1404
https://doi.org/10.1016/j.bbamcr.2017.05.008

Ma R, Zhang BW, Zhang ZB, Deng QJ (2020): LncRNA MALAT1 knockdown inhibits cell migration and invasion by suppressing autophagy through miR-384/GOLM1 axis in glioma. Eur. Rev. Med. Pharmacol. Sci. **24,** 2601-2615

Masri J, Bernath A, Martin J, Jo OD, Vartanian R, Funk A, Gera J (2007): mTORC2 activity is elevated in gliomas and promotes growth and cell motility via overexpression of rictor. Cancer Res. **67,** 11712-11720
https://doi.org/10.1158/0008-5472.CAN-07-2223

Minchenko OH, Kryvdiuk IV, Riabovol OO, Minchenko DO, Danilovskyi SV, Ratushna OO (2016): Inhibition of IRE1 modifies the hypoxic regulation of GADD family gene expressions in U87 glioma cells. Ukr. Biochem. J. **88,** 25-34
https://doi.org/10.15407/ubj88.02.025

Ostrom QT, Cote DJ, Ascha M, Kruchko C, Barnholtz-Sloan JS (2018): Adult glioma incidence and survival by race or ethnicity in the United States from 2000 to 2014. JAMA Oncol. **4,** 1254-1262

https://doi.org/10.1001/jamaoncol.2018.1789
Povey S, Lovering R, Bruford E, Wright M, Lush M, Wain H (2001): The HUGO Gene Nomenclature Committee (HGNC). Hum. Genet. **109,** 678-680 https://doi.org/10.1007/s00439-001-0615-0
Pucer A, Castino R, Mirković B, Falnoga I, Slejkovec Z, Isidoro C, Lah TT (2010): Differential role of cathepsins B and L in autophagy-associated cell death induced by arsenic trioxide in U87 human glioblastoma cells. Biol. Chem. **391,** 519-531 https://doi.org/10.1515/bc.2010.050
Ritchie ME, Phipson B, Wu D, Hu Y, Law CW, Shi W, Smyth GK (2015): limma powers differential expression analyses for RNA-sequencing and microarray studies. Nucleic. Acids. Res. **43,** e47 https://doi.org/10.1093/nar/gkv007
Shi L, Zhang W, Zou F, Mei L, Wu G, Teng Y (2016): KLHL21, a novel gene that contributes to the progression of hepatocellular carcinoma. BMC Cancer **16,** 815 https://doi.org/10.1186/s12885-016-2851-7
Shukla S, Patric IR, Patil V, Shwetha SD, Hegde AS, Chandramouli BA, Arivazhagan A, Santosh V, Somasundaram K (2014): Methylation silencing of ULK2, an autophagy gene, is essential for astrocyte transformation and tumor growth. J. Biol. Chem. **289,** 22306-22318 https://doi.org/10.1074/jbc.M114.567032
Song P, Yang S, Hua H, Zhang H, Kong Q, Wang J, Luo T, Jiang Y (2019): The regulatory protein GADD34 inhibits TRAIL-induced apoptosis via TRAF6/ERK-dependent stabilization of myeloid cell leukemia 1 in liver cancer cells. J. Biol. Chem. **294,** 5945-5955 https://doi.org/10.1074/jbc.RA118.006029
Tsuyuki S, Takabayashi M, Kawazu M, Kudo K, Watanabe A, Nagata Y, Kusama Y, Yoshida K (2014): Detection of WIPI1 mRNA as an indicator of autophagosome formation. Autophagy **10,** 497-513 https://doi.org/10.4161/auto.27419
Venkatesh HS, Chaumeil MM, Ward CS, Haas-Kogan DA, James CD, Ronen SM (2012): Reduced phosphocholine and hyperpolarized lactate provide magnetic resonance biomarkers of PI3K/Akt/mTOR inhibition in glioblastoma. Neuro. Oncol. **14,** 315-325 https://doi.org/10.1093/neuonc/nor209
Wang Y, Zhang X, Tang W, Lin Z, Xu L, Dong R, Li Y, Li J, Zhang Z, Li X, et al. (2017): miR-130a upregulates mTOR pathway by targeting TSC1 and is transactivated by NF-κB in high-grade serous ovarian carcinoma. Cell Death Differ. **24,** 2089-2100 https://doi.org/10.1038/cdd.2017.129
Wang J, Qi Q, Zhou W, Feng Z, Huang B, Chen A, Zhang D, Li W, Zhang Q, Jiang Z, et al. (2018): Inhibition of glioma growth by flavokawain B is mediated through endoplasmic reticulum stress induced autophagy. Autophagy **14,** 2007-2022 https://doi.org/10.1080/15548627.2018.1501133
Wang J, Ma J (2019): Integrated transcriptomic analysis of necrosis-related gene in diffuse gliomas. J. Neurol. Surg. A Cent. Eur. Neurosurg. **80,** 240-249 https://doi.org/10.1055/s-0039-1683448
Wang Y, Liu X, Guan G, Xiao Z, Zhao W, Zhuang M (2019a): Identification of a five-pseudogene signature for predicting survival and its ceRNA network in glioma. Front. Oncol. **9,** 1059 https://doi.org/10.3389/fonc.2019.01059
Wang Y, Liu X, Guan G, Zhao W, Zhuang M (2019b): A risk classification system with five-gene for survival prediction of glioblastoma patients. Front. Neurol. **10,** 745 https://doi.org/10.3389/fneur.2019.00745
Wang Z, Gao L, Guo X, Feng C, Lian W, Deng K, Xing B (2019c): Development and validation of a nomogram with an autophagy-related gene signature for predicting survival in patients with glioblastoma. Aging **11,** 12246-12269 https://doi.org/10.18632/aging.102566
Wang P, Zeng Z, Shen X, Tian X, Ye Q (2020a): Identification of a multi-RNA-type-based signature for recurrence-free survival prediction in patients with uterine corpus endometrial carcinoma. DNA Cell Biol. **39,** 615-630 https://doi.org/10.1089/dna.2019.5148
Wang QW, Liu HJ, Zhao Z, Zhang Y, Wang Z, Jiang T, Bao ZS (2020b): Prognostic correlation of autophagy-related gene expression-based risk signature in patients with glioblastoma. Onco. Targets Ther. **13,** 95-107 https://doi.org/10.2147/OTT.S238332
Wang Y, Zhao W, Xiao Z, Guan G, Liu X, Zhuang M (2020c): A risk signature with four autophagy-related genes for predicting survival of glioblastoma multiforme. J. Cell Mol. Med. **24,** 3807-3821 https://doi.org/10.1111/jcmm.14938
Wang C, Qiu J, Chen S, Li Y, Hu H, Cai Y, Hou L (2021): Prognostic model and nomogram construction based on autophagy signatures in lower grade glioma. J. Cell Physiol. **236,** 235-248 https://doi.org/10.1002/jcp.29837
Wu H, Zhu H, Liu DX, Niu TK, Ren X, Patel R, Hait WN, Yang JM (2009): Silencing of elongation factor-2 kinase potentiates the effect of 2-deoxy-D-glucose against human glioma cells through blunting of autophagy. Cancer Res. **69,** 2453-2460 https://doi.org/10.1158/0008-5472.CAN-08-2872
Wu F, Zhao Z, Chai R, Liu Y, Wang K, Wang Z, Li G, Huang R, Jiang H, Zhang K (2018): Expression profile analysis of antisense long non-coding RNA identifies WDFY3-AS2 as a prognostic biomarker in diffuse glioma. Cancer Cell Int. **18,** 107 https://doi.org/10.1186/s12935-018-0603-2
Wu F, Zhao Z, Chai RC, Liu YQ, Li GZ, Jiang HY, Jiang T (2019): Prognostic power of a lipid metabolism gene panel for diffuse gliomas. J. Cell Mol. Med. **23,** 7741-7748 https://doi.org/10.1111/jcmm.14647
Yang TQ, Lu XJ, Wu TF, Ding DD, Zhao ZH, Chen GL, Xie XS, Li B, Wei YX, Guo LC, et al. (2014): MicroRNA-16 inhibits glioma cell growth and invasion through suppression of BCL2 and the nuclear factor-κB1/MMP9 signaling pathway. Cancer Sci. **105,** 265-271 https://doi.org/10.1111/cas.12351
Yang N, Wang P, Wang WJ, Song YZ, Liang ZQ (2015): Inhibition of cathepsin L sensitizes human glioma cells to ionizing radiation in vitro through NF-κB signaling pathway. Acta Pharmacol. Sin. **36,** 400-410 https://doi.org/10.1038/aps.2014.148
Yang K, Niu L, Bai Y, Le W (2019): Glioblastoma: Targeting the autophagy in tumorigenesis. Brain Res. Bull. **153,** 334-340 https://doi.org/10.1016/j.brainresbull.2019.09.012

Zhang L, Zhang Y, Liu XY, Qin ZH, Yang JM (2011): Expression of elongation factor-2 kinase contributes to anoikis resistance and invasion of human glioma cells. Acta Pharmacol. Sin. **32,** 361-367 https://doi.org/10.1038/aps.2010.213

Zhang X, Wang X, Xu S, Li X, Ma X (2018): Cathepsin B contributes to radioresistance by enhancing homologous recombination in glioblastoma. Biomed. Pharmacother. **107,** 390-396 https://doi.org/10.1016/j.biopha.2018.08.007

Zhang GH, Zhong QY, Gou XX, Fan EX, Shuai Y, Wu MN, Yue GJ (2019): Seven genes for the prognostic prediction in patients with glioma. Clin. Transl. Oncol. **21,** 1327-1335 https://doi.org/10.1007/s12094-019-02057-3

Zhang Y, Liu Y, Liu H, Zhao Z, Wu F, Zeng F (2020): Clinical and biological significances of a methyltransferase-related signature in diffuse glioma. Front. Oncol. **10,** 508 https://doi.org/10.3389/fonc.2020.00508

Zhu WL, Tong H, Teh JT, Wang M (2014): Forkhead box protein O3 transcription factor negatively regulates autophagy in human cancer cells by inhibiting forkhead box protein O1 expression and cytosolic accumulation. Plos One **9,** e115087 https://doi.org/10.1371/journal.pone.0115087

Received: September 23, 2020
Final version accepted: March 22, 2021

doi: 10.4149/gpb_2021008

Supplementary Material

Identification of an autophagy-related 10-lncRNA-mRNA signature for distinguishing glioblastoma multiforme from lower-grade glioma and prognosis prediction

Bo Wei[1,*], Le Wang[2,*] and Jingwei Zhao[1]

[1] *Department of Neurosurgery, China-Japan Union Hospital of Jilin University, Changchun, Jilin, China*
[2] *Department of Ophthalmology, The First Hospital of Jilin University, Changchun, Jilin, China*

Supplementary table S1. The sample ID of TCGA and CGGA

Symbol	Symbol	Symbol	Symbol	Symbol	Symbol
CGGA_1473	TCGA-26-1442-01	CGGA_1386	TCGA-16-0846-01	CGGA_1634	TCGA-06-2557-01
CGGA_1443	TCGA-06-0129-01	CGGA_P156	TCGA-26-5134-01	CGGA_1502	TCGA-06-5410-01
CGGA_1065	TCGA-19-5960-01	CGGA_P399	TCGA-19-2625-01	CGGA_1559	TCGA-02-2483-01
CGGA_1003	TCGA-32-1980-01	CGGA_1208	TCGA-06-0238-01	CGGA_P520	TCGA-28-1747-01
CGGA_1744	TCGA-19-1390-01	CGGA_1595	TCGA-06-0750-01	CGGA_1617	TCGA-12-3653-01
CGGA_1649	TCGA-06-5417-01	CGGA_P17	TCGA-41-2571-01	CGGA_362	TCGA-16-1045-01
CGGA_1903	TCGA-19-2620-01	CGGA_290	TCGA-32-2615-01	CGGA_890	TCGA-06-2567-01
CGGA_P492	TCGA-32-1982-01	CGGA_1415	TCGA-06-0649-01	CGGA_1604	TCGA-28-2513-01
CGGA_P183	TCGA-06-0132-01	CGGA_1642	TCGA-06-5856-01	CGGA_1516	TCGA-06-0686-01
CGGA_1158	TCGA-06-0747-01	CGGA_1695	TCGA-06-2561-01	CGGA_P13	TCGA-12-0618-01
CGGA_1239	TCGA-27-1830-01	CGGA_903	TCGA-06-0645-01	CGGA_1647	TCGA-06-5858-01
CGGA_1675	TCGA-28-5216-01	CGGA_P122	TCGA-06-2565-01	CGGA_1863	TCGA-28-5218-01
CGGA_1627	TCGA-41-3915-01	CGGA_1551	TCGA-76-4926-01	CGGA_1517	TCGA-06-0138-01
CGGA_P177	TCGA-06-0219-01	CGGA_D28	TCGA-06-0139-01	CGGA_1640	TCGA-06-0210-01
CGGA_42	TCGA-32-1970-01	CGGA_1528	TCGA-06-0125-01	CGGA_1319	TCGA-06-5413-01
CGGA_1309	TCGA-06-5411-01	CGGA_103	TCGA-15-1444-01	CGGA_P150	TCGA-28-1753-01
CGGA_P131	TCGA-27-2523-01	CGGA_1413	TCGA-12-1597-01	CGGA_2081	TCGA-12-0821-01
CGGA_1211	TCGA-06-2570-01	CGGA_1383	TCGA-26-5139-01	CGGA_1127	TCGA-06-0130-01
CGGA_336	TCGA-06-5416-01	CGGA_P163	TCGA-06-0749-01	CGGA_P468	TCGA-06-0190-01
CGGA_1400	TCGA-06-0743-01	CGGA_869	TCGA-06-0744-01	CGGA_157	TCGA-27-2528-01
CGGA_810	TCGA-41-4097-01	CGGA_1232	TCGA-27-1837-01	CGGA_554	TCGA-41-2572-01
CGGA_1562	TCGA-19-2624-01	CGGA_P596	TCGA-12-0619-01	CGGA_1264	TCGA-41-5651-01
CGGA_J50	TCGA-06-0882-01	CGGA_P18	TCGA-26-5132-01	CGGA_P111	TCGA-19-2629-01
CGGA_P176	TCGA-02-0047-01	CGGA_P392	TCGA-26-5136-01	CGGA_P421	TCGA-76-4925-01
CGGA_P415	TCGA-06-1804-01	CGGA_1192	TCGA-27-1835-01	CGGA_1667	TCGA-08-0386-01
CGGA_P500	TCGA-32-4213-01	CGGA_2047	TCGA-06-5418-01	CGGA_P84	TCGA-14-0789-01
CGGA_P585	TCGA-06-2559-01	CGGA_P401	TCGA-14-0790-01	CGGA_1369	TCGA-12-3652-01
CGGA_1526	TCGA-06-0745-01	CGGA_1273	TCGA-06-0156-01	CGGA_1701	TCGA-27-1834-01
CGGA_320	TCGA-06-0878-01	CGGA_1164	TCGA-28-2514-01	CGGA_1554	TCGA-12-3650-01
CGGA_P7	TCGA-06-0178-01	CGGA_1368	TCGA-06-0158-01	CGGA_1592	TCGA-26-5135-01
CGGA_707	TCGA-14-1829-01	CGGA_1156	TCGA-06-0141-01	CGGA_P416	TCGA-19-2619-01
CGGA_P132	TCGA-12-5295-01	CGGA_1653	TCGA-06-0211-01	CGGA_P174	TCGA-06-0157-01
CGGA_1480	TCGA-06-0646-01	CGGA_1706	TCGA-32-2638-01	CGGA_P146	TCGA-28-5215-01
CGGA_P86	TCGA-28-5213-01	CGGA_1530	TCGA-02-2485-01	CGGA_P422	TCGA-27-2519-01

Supplementary table S1. The sample ID of TCGA and CGGA (continued)

Symbol	Symbol	Symbol	Symbol	Symbol	Symbol
CGGA_1103	TCGA-28-5204-01	CGGA_1546	TCGA-14-0787-01	CGGA_108	TCGA-S9-A7J1-01
CGGA_P270	TCGA-14-0781-01	CGGA_1183	TCGA-HT-A74L-01	CGGA_P311	TCGA-F6-A8O3-01
CGGA_1720	TCGA-06-0187-01	CGGA_1407	TCGA-FG-A4MX-01	CGGA_P182	TCGA-S9-A7R1-01
CGGA_1147	TCGA-06-0174-01	CGGA_1644	TCGA-P5-A5F6-01	CGGA_1191	TCGA-HT-7469-01
CGGA_1704	TCGA-76-4927-01	CGGA_1721	TCGA-HT-7873-01	CGGA_1655	TCGA-HT-7875-01
CGGA_1235	TCGA-06-2562-01	CGGA_135	TCGA-S9-A89V-01	CGGA_P337	TCGA-E1-A7YU-01
CGGA_1643	TCGA-02-0055-01	CGGA_P109	TCGA-FG-8186-01	CGGA_1345	TCGA-QH-A6CZ-01
CGGA_1504	TCGA-76-4928-01	CGGA_1689	TCGA-HT-7884-01	CGGA_1663	TCGA-FG-7641-01
CGGA_492	TCGA-27-2521-01	CGGA_1523	TCGA-E1-A7YW-01	CGGA_1496	TCGA-CS-5393-01
CGGA_1569	TCGA-06-5414-01	CGGA_P173	TCGA-DB-A64R-01	CGGA_1392	TCGA-TQ-A7RN-01
CGGA_1679	TCGA-32-2616-01	CGGA_1152	TCGA-HT-7692-01	CGGA_663	TCGA-CS-5394-01
CGGA_1513	TCGA-14-0871-01	CGGA_P144	TCGA-E1-5318-01	CGGA_1875	TCGA-FG-8182-01
CGGA_1786	TCGA-76-4931-01	CGGA_1037	TCGA-E1-A7YO-01	CGGA_194	TCGA-CS-6670-01
CGGA_P446	TCGA-32-5222-01	CGGA_1657	TCGA-HT-8564-01	CGGA_P512	TCGA-S9-A6TZ-01
CGGA_1747	TCGA-19-4065-01	CGGA_1630	TCGA-E1-A7YH-01	CGGA_881	TCGA-DB-5275-01
CGGA_809	TCGA-06-5412-01	CGGA_1539	TCGA-FG-8185-01	CGGA_1472	TCGA-DU-6396-01
CGGA_P143	TCGA-06-5859-01	CGGA_1488	TCGA-TQ-A7RG-01	CGGA_1404	TCGA-FG-A60K-01
CGGA_1534	TCGA-28-5209-01	CGGA_1658	TCGA-E1-A7YV-01	CGGA_1510	TCGA-DB-A64U-01
CGGA_1737	TCGA-15-0742-01	CGGA_1533	TCGA-S9-A7IY-01	CGGA_1771	TCGA-HW-7491-01
CGGA_1661	TCGA-12-5299-01	CGGA_P15	TCGA-HT-8114-01	CGGA_1912	TCGA-RY-A83X-01
CGGA_799	TCGA-32-2634-01	CGGA_901	TCGA-CS-6667-01	CGGA_1134	TCGA-HT-8107-01
CGGA_P364	TCGA-14-2554-01	CGGA_P269	TCGA-RY-A840-01	CGGA_1238	TCGA-DB-A64Q-01
CGGA_1536	TCGA-14-1823-01	CGGA_1181	TCGA-DH-A66F-01	CGGA_1402	TCGA-E1-5304-01
CGGA_1641	TCGA-06-0168-01	CGGA_P286	TCGA-QH-A6X4-01	CGGA_1524	TCGA-TQ-A7RV-01
CGGA_P16	TCGA-27-1832-01	CGGA_1568	TCGA-TQ-A7RO-01	CGGA_1718	TCGA-HW-8320-01
CGGA_P314	TCGA-28-5207-01	CGGA_634	TCGA-P5-A781-01	CGGA_1580	TCGA-R8-A6MK-01
CGGA_1169	TCGA-28-2509-01	CGGA_P27	TCGA-HT-7693-01	CGGA_1899	TCGA-DU-7007-01
CGGA_1087	TCGA-14-0817-01	CGGA_1728	TCGA-RY-A845-01	CGGA_1389	TCGA-HT-8113-01
CGGA_1723	TCGA-06-2563-01	CGGA_1985	TCGA-S9-A7QZ-01	CGGA_1714	TCGA-DU-7298-01
CGGA_265	TCGA-06-2564-01	CGGA_1303	TCGA-TQ-A7RQ-01	CGGA_P147	TCGA-VW-A7QS-01
CGGA_1433	TCGA-14-1825-01	CGGA_1256	TCGA-HT-7855-01	CGGA_P328	TCGA-DH-5141-01
CGGA_P137	TCGA-06-2569-01	CGGA_1416	TCGA-TQ-A7RI-01	CGGA_1659	TCGA-S9-A7R8-01
CGGA_P142	TCGA-26-5133-01	CGGA_2075	TCGA-HT-8012-01	CGGA_1586	TCGA-QH-A86X-01
CGGA_1377	TCGA-12-0616-01	CGGA_1731	TCGA-TQ-A7RR-01	CGGA_1286	TCGA-QH-A870-01
CGGA_1305	TCGA-27-2524-01	CGGA_625	TCGA-HT-7480-01	CGGA_1715	TCGA-HT-7688-01
CGGA_1566	TCGA-06-0184-01	CGGA_1212	TCGA-DU-A5TW-01	CGGA_1587	TCGA-DB-A75L-01
CGGA_1362	TCGA-06-2558-01	CGGA_1269	TCGA-S9-A7QY-01	CGGA_1427	TCGA-S9-A6WO-01
CGGA_1557	TCGA-28-5208-01	CGGA_P604	TCGA-DH-A7UV-01	CGGA_P19	TCGA-TM-A84Q-01
CGGA_D50	TCGA-19-1787-01	CGGA_1946	TCGA-S9-A7J2-01	CGGA_1626	TCGA-S9-A7QW-01
CGGA_1401	TCGA-27-2526-01	CGGA_1814	TCGA-TQ-A8XE-01	CGGA_279	TCGA-HT-7468-01
CGGA_1463	TCGA-02-2486-01	CGGA_P508	TCGA-DB-A64S-01	CGGA_P437	TCGA-DU-8164-01
CGGA_1552	TCGA-14-1034-01	CGGA_P298	TCGA-WY-A85D-01	CGGA_1571	TCGA-HW-7487-01
CGGA_1121	TCGA-27-1831-01	CGGA_P110	TCGA-QH-A6CW-01	CGGA_1155	TCGA-DB-A4XG-01
CGGA_165	TCGA-28-5220-01	CGGA_1575	TCGA-HT-7877-01	CGGA_P411	TCGA-DH-A66G-01
CGGA_P633	TCGA-32-2632-01	CGGA_1819	TCGA-P5-A5F0-01	CGGA_1318	TCGA-HW-8321-01
CGGA_P356	TCGA-76-4932-01	CGGA_288	TCGA-HT-7483-01	CGGA_1066	TCGA-P5-A77X-01
CGGA_P103	TCGA-06-5408-01	CGGA_1291	TCGA-HT-8108-01	CGGA_1440	TCGA-DU-A6S2-01
CGGA_1882	TCGA-76-4929-01	CGGA_P93	TCGA-HT-7874-01	CGGA_724	TCGA-TM-A84L-01
CGGA_2079	TCGA-06-0644-01	CGGA_1482	TCGA-DB-A4XC-01	CGGA_1260	TCGA-VV-A829-01

Supplementary table S1. The sample ID of TCGA and CGGA (continued)

Symbol	Symbol
CGGA_1471	TCGA-DH-A7UT-01
CGGA_P310	TCGA-DU-A7TG-01
CGGA_1339	TCGA-DU-A6S6-01
CGGA_1880	TCGA-HT-7879-01
CGGA_1131	TCGA-DB-A4XD-01
CGGA_P438	TCGA-S9-A6TV-01
CGGA_1321	TCGA-DU-5849-01
CGGA_1162	TCGA-S9-A6TX-01
CGGA_1097	TCGA-S9-A7J3-01
CGGA_P179	TCGA-DU-5870-01
CGGA_1716	TCGA-HT-7681-01
CGGA_P28	TCGA-FG-7637-01
CGGA_1431	TCGA-HT-A618-01
CGGA_1620	TCGA-HW-8319-01
CGGA_P505	TCGA-DU-A76O-01
CGGA_P568	TCGA-HT-A61B-01
CGGA_1703	TCGA-WY-A85A-01
CGGA_1725	TCGA-TM-A84R-01
CGGA_621	TCGA-DU-A5TS-01
CGGA_1955	TCGA-FG-8189-01
CGGA_P5	TCGA-TQ-A7RH-01
CGGA_1594	TCGA-DU-8166-01
CGGA_1161	TCGA-HW-7495-01
CGGA_1041	TCGA-S9-A7R7-01
CGGA_1361	TCGA-RY-A83Y-01
CGGA_1688	TCGA-E1-5305-01
CGGA_1994	TCGA-VM-A8C8-01
CGGA_P439	TCGA-DH-A66B-01
CGGA_1501	TCGA-DU-8168-01
CGGA_721	TCGA-DU-7009-01
CGGA_1036	TCGA-E1-A7Z6-01
CGGA_1525	TCGA-TM-A84H-01
CGGA_1662	TCGA-S9-A6U8-01
CGGA_509	TCGA-W9-A837-01
CGGA_1452	TCGA-P5-A5F4-01
CGGA_1441	TCGA-TQ-A7RV-02
CGGA_1902	TCGA-P5-A730-01
CGGA_P199	TCGA-HT-7610-01
CGGA_1648	TCGA-P5-A780-01
CGGA_P151	TCGA-DU-A76R-01
CGGA_1207	TCGA-S9-A7IQ-01
CGGA_1690	TCGA-VM-A8CE-01
CGGA_P145	TCGA-DB-A75M-01
CGGA_1735	TCGA-S9-A6U2-01
CGGA_1739	TCGA-HT-7856-01
CGGA_P155	TCGA-HT-8109-01
CGGA_106	TCGA-CS-6666-01
CGGA_1508	TCGA-DH-A7US-01
CGGA_1671	TCGA-RY-A843-01
CGGA_P315	TCGA-VM-A8CB-01
CGGA_P181	TCGA-HT-7482-01
CGGA_P501	TCGA-HT-7477-01
CGGA_P358	TCGA-HT-7609-01
CGGA_1417	TCGA-DB-A75K-01
CGGA_882	TCGA-VM-A8CF-01
CGGA_P335	TCGA-FN-7833-01
CGGA_1018	TCGA-E1-5307-01
CGGA_1850	TCGA-HT-7478-01
CGGA_1736	TCGA-E1-A7YE-01
CGGA_1398	TCGA-DU-A7T8-01
CGGA_1178	TCGA-E1-A7YS-01
CGGA_1857	TCGA-HT-7881-01
CGGA_P346	TCGA-DU-6542-01
CGGA_1527	TCGA-DU-7302-01
CGGA_1618	TCGA-DB-A4XF-01
CGGA_1492	TCGA-HT-8111-01
CGGA_1901	TCGA-HW-A5KJ-01
CGGA_1906	TCGA-DU-6408-01
CGGA_1487	TCGA-E1-5319-01
CGGA_1623	TCGA-S9-A6TS-01
CGGA_P185	TCGA-P5-A5EV-01
CGGA_1598	TCGA-FG-5965-01
CGGA_1686	TCGA-FG-A4MY-01
CGGA_P31	TCGA-FG-A70Y-01
CGGA_1854	TCGA-TQ-A7RW-01
CGGA_1410	TCGA-DU-A7TA-01
CGGA_1645	TCGA-TM-A84T-01
CGGA_P483	TCGA-E1-A7Z4-01
CGGA_P21	TCGA-HT-7880-01
CGGA_1058	TCGA-WY-A85B-01
CGGA_1565	TCGA-FG-6689-01
CGGA_1669	TCGA-HT-A5RB-01
CGGA_P83	TCGA-FG-8187-01
CGGA_P316	TCGA-TM-A84I-01
CGGA_1700	TCGA-P5-A5EZ-01
CGGA_1335	TCGA-FG-6690-01
CGGA_1591	TCGA-HT-7472-01
CGGA_730	TCGA-S9-A6U6-01
CGGA_1055	TCGA-QH-A6CY-01
CGGA_P20	TCGA-DU-6397-01
CGGA_1543	TCGA-EZ-7264-01
CGGA_867	TCGA-QH-A65V-01
CGGA_1535	TCGA-S9-A6U9-01
CGGA_1184	TCGA-TQ-A7RJ-01
CGGA_1727	TCGA-VM-A8CH-01
CGGA_1673	TCGA-DB-A4XB-01
CGGA_1132	TCGA-HT-7677-01
CGGA_P106	TCGA-R8-A6ML-01
CGGA_1126	TCGA-E1-A7YM-01
CGGA_457	TCGA-P5-A72X-01
CGGA_1505	TCGA-HT-7690-01
CGGA_1477	TCGA-DB-A64X-01
CGGA_521	TCGA-TQ-A7RF-01
CGGA_1589	TCGA-HT-7604-01
CGGA_P385	TCGA-HW-A5KL-01
CGGA_P510	TCGA-DB-5270-01
CGGA_1033	TCGA-WY-A858-01
CGGA_1159	TCGA-IK-8125-01
CGGA_1451	TCGA-CS-6669-01
CGGA_888	TCGA-S9-A6WD-01
CGGA_1826	TCGA-E1-5311-01
CGGA_P279	TCGA-TM-A84S-01
CGGA_1693	TCGA-HT-7473-01
CGGA_1017	TCGA-DU-7309-01
CGGA_P388	TCGA-HT-7694-01
CGGA_P98	TCGA-IK-7675-01
CGGA_1750	TCGA-TM-A84G-01
CGGA_1455	TCGA-TM-A7CF-01
CGGA_1434	TCGA-S9-A7IZ-01
CGGA_1579	TCGA-DU-A5TR-01
CGGA_705	TCGA-HT-A615-01
CGGA_2046	TCGA-HT-8013-01
CGGA_530	TCGA-WY-A859-01
CGGA_1597	TCGA-P5-A5F2-01
CGGA_1371	TCGA-TM-A84M-01
CGGA_1425	TCGA-WY-A85C-01
CGGA_1421	TCGA-HT-A5R7-01
CGGA_1403	TCGA-E1-5322-01
CGGA_482	TCGA-HT-7858-01
CGGA_P102	TCGA-R8-A73M-01
CGGA_1608	TCGA-DH-A66D-01
CGGA_1057	TCGA-DU-6400-01
CGGA_P157	TCGA-HT-A5R5-01
CGGA_1866	TCGA-S9-A6U1-01
CGGA_503	TCGA-DU-7304-01
CGGA_1106	TCGA-QH-A65Z-01
CGGA_1601	TCGA-FG-A710-01
CGGA_P326	TCGA-DU-5871-01
CGGA_P99	TCGA-HT-7481-01
CGGA_1664	TCGA-S9-A6TY-01
CGGA_1108	TCGA-DU-8163-01
CGGA_2008	TCGA-HT-7689-01
CGGA_1458	TCGA-HT-8105-01
CGGA_2002	TCGA-S9-A6WH-01
CGGA_P121	TCGA-DU-A7TI-01
CGGA_1606	TCGA-HT-A61A-01
CGGA_862	TCGA-HT-7474-01

Supplementary table S1. The sample ID of TCGA and CGGA (continued)

Symbol	Symbol	Symbol	Symbol	Symbol	Symbol
CGGA_2078	TCGA-FG-7634-01	CGGA_P153	TCGA-DU-7008-01	CGGA_P306	TCGA-FG-7638-01
CGGA_1420	TCGA-DU-7019-01	CGGA_1614	TCGA-P5-A5EX-01	CGGA_1457	TCGA-HW-7489-01
CGGA_1687	TCGA-DB-5281-01	CGGA_P11	TCGA-QH-A65S-01	CGGA_1553	TCGA-DB-A4XH-01
CGGA_1447	TCGA-HT-7601-01	CGGA_1840	TCGA-HT-7695-01	CGGA_1491	TCGA-HT-8018-01
CGGA_1621	TCGA-FG-8181-01	CGGA_780	TCGA-HT-7854-01	CGGA_568	TCGA-HT-7676-01
CGGA_1583	TCGA-VM-A8CA-01	CGGA_P89	TCGA-CS-4944-01	CGGA_1548	TCGA-DB-A75P-01
CGGA_1680	TCGA-E1-A7YY-01	CGGA_1833	TCGA-DU-5870-02	CGGA_1770	TCGA-DH-5142-01
CGGA_1048	TCGA-E1-A7YK-01	CGGA_J73	TCGA-FG-8191-01	CGGA_1694	TCGA-P5-A72W-01
CGGA_2006	TCGA-QH-A6X9-01	CGGA_1295	TCGA-TM-A7C4-01	CGGA_P164	TCGA-DU-7294-01
CGGA_1811	TCGA-S9-A6WI-01	CGGA_P128	TCGA-DB-A64P-01	CGGA_1743	TCGA-HT-7606-01
CGGA_1148	TCGA-FG-8188-01	CGGA_1563	TCGA-P5-A5EW-01	CGGA_1607	TCGA-DU-8162-01
CGGA_703	TCGA-HT-8019-01	CGGA_1541	TCGA-S9-A7QX-01	CGGA_358	TCGA-DU-5853-01
CGGA_1300	TCGA-E1-A7Z3-01	CGGA_1350	TCGA-S9-A6WQ-01	CGGA_1815	TCGA-DU-A6S3-01
CGGA_107	TCGA-S9-A6WE-01	CGGA_861	TCGA-QH-A65R-01	CGGA_1870	TCGA-TQ-A7RK-01
CGGA_P619	TCGA-HW-8322-01	CGGA_1697	TCGA-HT-7607-01	CGGA_1624	TCGA-QH-A6X5-01
CGGA_1317	TCGA-P5-A731-01	CGGA_1032	TCGA-DB-A4XA-01	CGGA_1558	TCGA-DU-6403-01
CGGA_1650	TCGA-DU-7015-01	CGGA_1507	TCGA-HT-A4DV-01	CGGA_487	TCGA-FG-A4MT-02
CGGA_1467	TCGA-TM-A7CA-01	CGGA_1953	TCGA-DB-A64V-01	CGGA_P100	TCGA-CS-5396-01
CGGA_1764	TCGA-DH-5143-01	CGGA_1426	TCGA-HT-7620-01	CGGA_1454	TCGA-HT-7479-01
CGGA_652	TCGA-DU-6401-01	CGGA_P112	TCGA-QH-A6XA-01	CGGA_1702	TCGA-DH-A7UU-01
CGGA_1605	TCGA-FG-6691-01	CGGA_1740	TCGA-FG-5962-01	CGGA_825	TCGA-HT-8563-01
CGGA_1154	TCGA-P5-A5F1-01	CGGA_P30	TCGA-S9-A6WN-01	CGGA_2115	TCGA-P5-A735-01
CGGA_P295	TCGA-TM-A7CF-02	CGGA_1685	TCGA-HT-7475-01	CGGA_P22	TCGA-HT-7691-01
CGGA_1785	TCGA-S9-A7R3-01	CGGA_1613	TCGA-HT-7470-01	CGGA_P461	TCGA-HT-7680-01
CGGA_1135	TCGA-QH-A6CU-01	CGGA_1337	TCGA-HT-8558-01	CGGA_406	TCGA-RY-A83Z-01
CGGA_1612	TCGA-DU-7011-01	CGGA_474	TCGA-HW-7493-01	CGGA_1228	TCGA-HT-7603-01
CGGA_1157	TCGA-S9-A6TW-01	CGGA_507	TCGA-E1-5303-01	CGGA_1537	TCGA-DU-7010-01
CGGA_1195	TCGA-DU-A7TC-01	CGGA_1862	TCGA-S9-A6WL-01	CGGA_1390	TCGA-DB-A75O-01
CGGA_1776	TCGA-DB-A4X9-01	CGGA_P319	TCGA-DU-6395-01	CGGA_1359	TCGA-TM-A7C5-01
CGGA_2129	TCGA-HT-8010-01	CGGA_1886	TCGA-HT-A614-01	CGGA_1462	TCGA-HT-7467-01
CGGA_1567	TCGA-KT-A74X-01	CGGA_1446	TCGA-HW-7490-01	CGGA_1619	TCGA-P5-A733-01
CGGA_112	TCGA-TQ-A7RK-02	CGGA_2024	TCGA-DU-7014-01	CGGA_2003	TCGA-HW-A5KM-01
CGGA_P160	TCGA-DB-5279-01	CGGA_P172	TCGA-E1-5302-01	CGGA_1459	TCGA-FG-7643-01
CGGA_1972	TCGA-QH-A6X8-01	CGGA_1610	TCGA-TM-A84F-01	CGGA_1437	TCGA-HT-A74O-01
CGGA_1012	TCGA-DU-A5TU-01	CGGA_28	TCGA-TQ-A8XE-02	CGGA_1745	TCGA-HT-7485-01
CGGA_1356	TCGA-S9-A6U5-01	CGGA_831	TCGA-CS-6290-01	CGGA_1588	TCGA-DU-6394-01
CGGA_1560	TCGA-HT-7605-01	CGGA_1699	TCGA-HT-A616-01	CGGA_1615	TCGA-FG-A60J-01
CGGA_1204	TCGA-HT-A74J-01	CGGA_720	TCGA-FG-A4MT-01	CGGA_1817	TCGA-FG-A60L-01
CGGA_P594	TCGA-RY-A847-01	CGGA_1391	TCGA-HT-7686-01	CGGA_1500	TCGA-S9-A6TU-01
CGGA_889	TCGA-DU-A6S7-01	CGGA_P87	TCGA-DB-A64W-01	CGGA_1538	TCGA-FG-A711-01
CGGA_D19	TCGA-P5-A737-01	CGGA_P113	TCGA-FG-A713-01	CGGA_2062	TCGA-HT-7608-01
CGGA_1435	TCGA-HT-7611-01	CGGA_1670	TCGA-S9-A7R4-01	CGGA_1908	TCGA-CS-6188-01
CGGA_1111	TCGA-DU-5855-01	CGGA_1141	TCGA-DB-5278-01	CGGA_1698	TCGA-S9-A6WG-01
CGGA_1334	TCGA-DU-7300-01	CGGA_1544	TCGA-HT-7476-01	CGGA_139	TCGA-FG-A6J1-01
CGGA_1769	TCGA-DB-5280-01	CGGA_1429	TCGA-DU-6393-01	CGGA_1469	TCGA-CS-4938-01
CGGA_1660	TCGA-DB-A4XE-01	CGGA_1130	TCGA-F6-A8O4-01	CGGA_1521	TCGA-CS-4942-01
CGGA_1223	TCGA-VV-A86M-01	CGGA_P609	TCGA-HT-7902-01	CGGA_1474	TCGA-HT-7687-01
CGGA_P625	TCGA-DB-A64L-01	CGGA_883	TCGA-DU-7299-01	CGGA_1424	TCGA-P5-A5EY-01
CGGA_1738	TCGA-TM-A84O-01	CGGA_420	TCGA-DU-5872-01	CGGA_1729	TCGA-HW-7486-01

Supplementary table S1. The sample ID of TCGA and CGGA (continued)

Symbol	Symbol
CGGA_1529	TCGA-DU-8167-01
CGGA_777	TCGA-WH-A86K-01
CGGA_1865	TCGA-DH-5144-01
CGGA_P308	TCGA-HT-7471-01
CGGA_1829	TCGA-S9-A7J0-01
CGGA_1708	TCGA-QH-A6X3-01
CGGA_1382	TCGA-HT-8015-01
CGGA_846	TCGA-DU-6399-01
CGGA_763	TCGA-CS-6668-01
CGGA_1326	TCGA-E1-A7Z2-01
CGGA_369	TCGA-DU-6407-01
CGGA_1631	TCGA-WY-A85E-01
CGGA_1651	TCGA-HT-7602-01
CGGA_P280	TCGA-TM-A7C3-01
CGGA_619	TCGA-FG-7636-01
CGGA_1520	TCGA-DU-A5TP-01
CGGA_1758	TCGA-FG-5964-01
CGGA_887	TCGA-QH-A65X-01
CGGA_2053	TCGA-HT-7684-01
CGGA_P338	TCGA-S9-A89Z-01
CGGA_1809	TCGA-R8-A6MO-01
CGGA_1172	TCGA-DU-7306-01
CGGA_1572	TCGA-E1-A7YN-01
CGGA_1236	TCGA-DU-A76K-01
CGGA_1713	TCGA-DU-5872-02
CGGA_1596	TCGA-P5-A77W-01
CGGA_1418	TCGA-P5-A736-01
CGGA_P283	TCGA-DH-5140-01
CGGA_583	TCGA-DB-5273-01
CGGA_1682	TCGA-VM-A8CD-01
CGGA_1030	TCGA-DU-A7TD-01
CGGA_852	TCGA-S9-A6WP-01
CGGA_1226	TCGA-DU-A7TB-01
CGGA_P271	TCGA-DU-7292-01
CGGA_2013	TCGA-FG-A87Q-01
CGGA_1760	TCGA-DU-7301-01
CGGA_1518	TCGA-HT-A5RC-01
CGGA_2121	TCGA-DU-A6S8-01
CGGA_1002	TCGA-CS-4941-01
CGGA_863	TCGA-DU-6404-01
CGGA_1444	TCGA-FG-A4MU-01
CGGA_1014	TCGA-DU-8161-01
CGGA_1205	TCGA-DU-7018-01

Symbol	Symbol
CGGA_1311	TCGA-FG-5965-02
CGGA_P108	TCGA-CS-5395-01
CGGA_1010	TCGA-S9-A7R2-01
CGGA_1791	TCGA-DU-6397-02
CGGA_1773	TCGA-DU-6407-02
CGGA_1478	TCGA-FG-A87N-01
CGGA_1142	TCGA-S9-A7IX-01
CGGA_1144	TCGA-TM-A84C-01
CGGA_1603	TCGA-HT-8110-01
CGGA_1051	TCGA-S9-A6UA-01
CGGA_1749	TCGA-HW-A5KK-01
CGGA_2056	TCGA-S9-A6UB-01
CGGA_1354	TCGA-HT-7860-01
CGGA_1419	TCGA-HT-A617-01
CGGA_1911	TCGA-DU-5854-01
CGGA_1635	TCGA-DU-6402-01
CGGA_P266	TCGA-HT-7882-01
CGGA_P158	TCGA-HT-A74K-01
CGGA_1075	TCGA-FG-A6IZ-01
CGGA_2106	TCGA-HT-A619-01
CGGA_1514	TCGA-DU-6392-01
CGGA_1257	TCGA-DB-5277-01
CGGA_1430	TCGA-TM-A84B-01
CGGA_1812	TCGA-DU-A5TT-01
CGGA_1461	TCGA-QH-A6CS-01
CGGA_P165	TCGA-CS-5397-01
CGGA_1100	TCGA-QH-A6CV-01
CGGA_1380	TCGA-QH-A6CX-01
CGGA_1681	TCGA-DU-7012-01
CGGA_1185	TCGA-DU-A5TY-01
CGGA_1248	TCGA-DU-6404-02
CGGA_1820	TCGA-TQ-A7RP-01
CGGA_P159	TCGA-E1-A7YD-01
CGGA_P104	TCGA-DU-7013-01
CGGA_1976	TCGA-HT-A4DS-01
CGGA_1365	TCGA-HT-8104-01
CGGA_1611	TCGA-FG-A70Z-01
CGGA_1387	TCGA-HT-A61C-01
CGGA_1542	TCGA-VM-A8C9-01
CGGA_1255	TCGA-KT-A7W1-01
CGGA_1497	TCGA-TM-A84J-01
CGGA_1137	TCGA-E1-A7YQ-01
CGGA_1138	TCGA-HT-8011-01

Symbol	Symbol
CGGA_1476	TCGA-DU-5874-01
CGGA_1101	TCGA-DU-8158-01
CGGA_P178	TCGA-DU-7290-01
CGGA_1198	TCGA-HT-7857-01
CGGA_1353	TCGA-DU-A7TJ-01
CGGA_1481	TCGA-FG-5963-01
CGGA_1807	TCGA-HT-A5RA-01
CGGA_1262	TCGA-S9-A6WM-01
CGGA_1378	TCGA-DU-6410-01
CGGA_P29	TCGA-DB-A64O-01
CGGA_P25	TCGA-DH-A7UR-01
CGGA_1666	TCGA-CS-4943-01
CGGA_P115	TCGA-DU-6406-01
CGGA_P610	TCGA-FG-6688-01
CGGA_1120	TCGA-VW-A8FI-01
CGGA_1696	TCGA-HT-A74H-01
CGGA_1709	TCGA-E1-A7YJ-01
CGGA_1503	TCGA-DU-7006-01
CGGA_1656	TCGA-HT-7616-01
CGGA_1678	TCGA-S9-A6U0-01
CGGA_P175	TCGA-FG-A4MW-01
CGGA_P136	TCGA-DU-5847-01
CGGA_P116	TCGA-E1-A7YL-01
CGGA_120	TCGA-HT-A5R9-01
CGGA_1086	TCGA-TQ-A7RM-01
CGGA_1422	TCGA-DU-6405-01
CGGA_1445	TCGA-DB-5274-01
CGGA_P3	TCGA-FG-5963-02
CGGA_1494	TCGA-QH-A6XC-01
CGGA_1780	TCGA-DU-A7T6-01
CGGA_1722	TCGA-P5-A72Z-01
CGGA_1282	TCGA-CS-6186-01
CGGA_P265	TCGA-DU-5852-01
CGGA_P23	TCGA-P5-A72U-01
CGGA_1767	TCGA-E1-A7YI-01
CGGA_P180	TCGA-S9-A7IS-01
CGGA_1486	TCGA-DU-8165-01
CGGA_P205	TCGA-DU-A76L-01
CGGA_1564	TCGA-DU-7304-02
	TCGA-DH-A669-01
	TCGA-FG-6692-01
	TCGA-FG-A6J3-01
	TCGA-DH-A669-02

Supplementary table S2. PCA result

		PC1	PC2	PC3	PC4	PC5	PC6	PC7	PC8	PC9	PC10
CGGA	Standard deviation	3.1428	0.24215	0.13171	0.11793	0.10335	0.08359	0.08156	0.06177	0.05141	0.04711
	Proportion of Variance	0.9877	0.00586	0.00173	0.00139	0.00107	0.00070	0.00067	0.00038	0.00026	0.00022
	Cumulative Proportion	0.9877	0.99357	0.99531	0.99670	0.99777	0.99847	0.99913	0.99951	0.99978	1.00000
TCGA	Standard deviation	1.7676	1.4681	1.0854	0.91227	0.89266	0.7497	0.67143	0.6115	0.53706	0.48771
	Proportion of Variance	0.3125	0.2155	0.1178	0.08322	0.07968	0.0562	0.04508	0.0374	0.02884	0.02379
	Cumulative Proportion	0.8125	0.8280	0.8458	0.82900	0.90869	0.9149	0.92997	0.9474	0.97621	0.02379